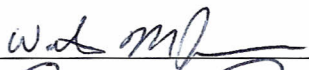


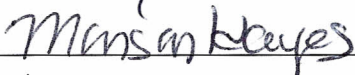
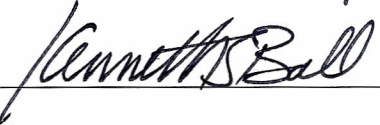


MULTI-RATE STATE-DEPENDENT PRIMITIVES UNDERLIE THE MOTOR ADAPTATION  
AND UNLEARNING OF MOTION-DEPENDENT FORCE PERTURBATIONS

by

Eghbal Hosseini Asl  
A Thesis  
Submitted to the  
Graduate Faculty  
of  
George Mason University  
In Partial fulfillment of  
The Requirements for the Degree  
of  
Master of Science  
Electrical Engineering

Committee:

 _____	Dr. Wilsaan M. Joiner, Thesis Director
 _____	Dr. Janos Gertler, Committee Member
 _____	Dr. Gerald Cook, Committee Member
 _____	Dr. Manson Hayes, Chairman, Department of Electrical and Computer Engineering
 _____	Dr. Kenneth S. Ball, Associate Dean for Research and Graduate Studies

Date: December 29, 2014 Fall Semester 2014  
George Mason University  
Fairfax, VA

Multi-rate State-dependent Primitives Underlie The Motor Adaptation and Unlearning to  
Motion-Dependent Force Perturbations

A thesis submitted in partial fulfillment of the requirements for the degree of  
Master of Science at George Mason University

By

Eghbal Hosseini Asl  
Bachelor of Science  
Iran University of Science and Technology, 2010

Director: Dr. Wilsaan M. Joiner, Professor  
Department of Electrical and Computer Engineering

Fall Semester 2014  
George Mason University  
Fairfax, VA

Copyright © 2014 by Eghbal Hosseini Asl  
All Rights Reserved

## Acknowledgments

I would like to thank my advisor, my family and many friends who have help me made this happen.

First I would like to thank my committee members Professor Janos Gertler and Professor Gerald Cook for their helpful insights and supportive feedback.

I would like to thank my thesis advisor Dr. Wilsaan Joiner, for his help and support at every stage of my work. Since the first day I started working with him in January 2013, each day has been an adventure and a new learning experience. He has taught me how to think critically in science, and helped me improving my writing and presentation techniques. Most importantly he implanted his passion for doing good science in me, without which I would not be here. He has also been a good friend to me, in making hard decisions and going forward.

I would also like to thank members of Sensorimotor Integration Lab for sharing their life with me. To my fellow graduate students (Sonia Bansal, Krthik Murthy), Undergraduate students (Katrina Nguyen, Laith Alhussain, Justin Sellman) and postdoc (Laurence Bray) I enjoy every day in the lab working with you. I specially want to thank Katrina for all her help and never giving up even when 'the cat was on the roof'. I could always count on Sonia for Saxbys trips which always accompanied with interesting conversations and debates, and often overhauling manuscripts. It is a privilege to have you as friends.

# Table of Contents

	Page
List of Figures . . . . .	vi
Abstract . . . . .	viii
1 Chapter One . . . . .	1
1.1 Multiple Rates of Motor Adaptation . . . . .	2
1.2 Viscoelastic Primitives for Motor Adaptation . . . . .	3
2 Chapter Two . . . . .	6
2.1 Introduction . . . . .	6
2.2 Methods . . . . .	7
2.2.1 Participants . . . . .	7
2.2.2 Experimental setup . . . . .	8
2.2.3 Task . . . . .	11
2.2.4 Analysis of Force Profiles . . . . .	12
2.3 Results . . . . .	13
2.3.1 Adaptive Responses to a Position- and Velocity-Dependent Force-field	13
2.3.2 Gain-Space Analysis of Adaptive Responses to Single State Force-fields	16
2.3.3 Gain-Space Analysis of Combination Force-Field . . . . .	20
2.3.4 Comparison of Unlearning Behavior Between Different Force-field En-	
vironments . . . . .	23
2.4 Discussion . . . . .	26
2.4.1 Previous Studies of Unlearning of Motor Memory . . . . .	27
2.4.2 Neural Correlates of Motion-dependent States in Motor System . . .	28
3 Chapter Three . . . . .	31
3.1 Introduction . . . . .	31
3.2 Multi-rate Model of Motor Adaptation . . . . .	32
3.2.1 Response Characteristics of Multi-rate Model of Motor Adaptation	
to Force-fields . . . . .	33
3.3 Viscoelastic Primitive Model for Motor Adaptation . . . . .	35

3.3.1	Simulation of Viscoelastic Model in Force-field Adaptation and Un-learning . . . . .	39
3.4	Multi-rate State-dependent Primitive Model for Motor Adaptation . . . . .	44
3.4.1	Multi-rate State-dependent Primitive Model with Same Distribution	45
3.4.2	Multi-rate state-dependent primitive model with distinct distributions	50
3.5	Discussion . . . . .	56
3.5.1	Two Rates models of Motor Adaptation . . . . .	56
3.5.2	Asymmetries in the Primitive Distributions . . . . .	57
4	Chapter Four . . . . .	58
4.1	Introduction . . . . .	58
4.2	Prediction of Multi-rate State-dependent Primitive Model During Gradual Introduction of the Force-field . . . . .	58
4.3	Prediction of Multi-rate State-dependent Primitive Model During Extended Exposure to the Force-field . . . . .	59
	Bibliography . . . . .	63

## List of Figures

Figure	Page
2.1 Experimental design . . . . .	10
2.2 Evolution of learning during adaptation and unlearning of the position and velocity-FF . . . . .	15
2.3 Gain space representation of the adaptation and unlearning of the position and velocity-FF . . . . .	18
2.4 Gain space representation of combination force-field adaptation and unlearning	21
2.5 Gain space representation of position-biased force-field adaptation and unlearning . . . . .	24
2.6 Comparison between the decay of motion-dependent force states for different force-field environments . . . . .	25
3.1 Multi-rate model of motor adaptation . . . . .	33
3.2 Adaptation and unlearning of force-field in two-rate model . . . . .	34
3.3 Evolution of the fast and slow states in the multi-rate model . . . . .	36
3.4 Viscoelastic primitive model for motor adaptation . . . . .	38
3.5 Combination of the movement variables in each primitive . . . . .	38
3.6 Simulation of viscoelastic primitive model in position and velocity FFs . . .	41
3.7 Simulation of viscoelastic primitive model in a combination-FF . . . . .	42
3.8 Simulation of viscoelastic primitive model in a position biased-FF . . . . .	43
3.9 Simulation multi-rate state-dependent primitive model with same distribution in the position and velocity-FFs . . . . .	47
3.10 Simulation multi-rate state-dependent primitive model with same distribution in the combination-FF . . . . .	48
3.11 Simulation multi-rate state-dependent primitive model with same distribution in the position-biased-FF . . . . .	49
3.12 Simulation of multi-rate state-dependent primitive model with distinct distributions in the position and velocity-FFs . . . . .	52
3.13 Simulation multi-rate state-dependent primitive model with different distribution in combination-FF . . . . .	53

3.14	Simulation multi-rate state-dependent primitive model with different distribution in position-biased FF . . . . .	54
3.15	Evolution slow and fast states in multi-rate state-dependent primitive model for the combination-FF . . . . .	55
3.16	Evolution slow and fast states in multi-rate state-dependent primitive model for the position-biased-FF . . . . .	55
4.1	Simulation multi-rate state-dependent primitive model with different distribution in gradual position-FF and velocity-FF . . . . .	60
4.2	Simulation multi-rate state-dependent primitive model with distinct distributions in the extended exposure position-FF . . . . .	62



## Abstract

MULTI-RATE STATE-DEPENDENT PRIMITIVES UNDERLIE THE MOTOR ADAP-  
TATION AND UNLEARNING TO MOTION-DEPENDENT FORCE PERTURBATIONS

Eghbal Hosseini Asl

George Mason University, 2014

Thesis Director: Dr. Wilsaan M. Joiner

The motor system can compensate for perturbations to the body and within the environment through experience. Motor adaptation studies have suggested that this compensation takes place by developing and updating of an internal model of the body and environment. Previous research has examined the time-scales, learning primitives, and stability of the motor memory following adaptation to forces dependent on motion kinematics. However, computational models that simultaneously capture these aspects of motor adaptation are lacking. In this thesis, we propose a model that encompasses different features of adaptation to motion-dependent force-fields. We first trained human subjects in different force-field environments and measured the adaptation and subsequent unlearning. We then formulated a motor-adaptation model that takes into account both the motion-dependency and time-scales of motor memory, and investigated its ability to explain several characteristics of experimental finding, including the hysteresis between adaptation and unlearning, and motion-dependent adaptation asymmetries.

We finally use the new model to predict the motor adaptation behavior under gradual introduction of the perturbation, as well as savings upon re-exposure to perturbation after a period of inactivity.

## Chapter 1:

Species have evolved from single cells passively responding to the environment to multicellular organisms actively interacting with it. Humans, as a multicellular organism, have surpassed the others in cognitive abilities and are able to utilize their motor system to mold the objects and develop tools that can exploit the resources in the environment. When building a new object, for example, our hands perform a synchronous sequence of motions which is hardly achievable by any other species or even most advanced robotic technology.

The complexity of motor system is manifested in two domains. First, through practice, humans are able to learn an infinite range of movement sequences. Newborn babies make their first steps to explore the world after months of practice to maintain the balance while standing and synchronizing their steps. Ballet dancers, on the other hand, move their body in harmonious sequences and transform movement into a form of art. Second, once a movement pattern is learned, humans are able to encode this pattern into memories that last for days, months, or even a lifetime. A newborn baby who has learned to walk will never forget pattern of limb motion in walking.

Understanding the basis for learning and retaining the memories of movements in the central nervous system has been baffling scientists over a century. An array of experiments and approaches have been applied to reveal the neural basis of motor learning and memory, including recording of neurons involved in limb motion in both healthy and unhealthy brains, behavioral experiments, as well as computational approaches. Both Behavioral and computational approaches have been successful in explaining many aspects of motor learning and memory [1–4]. These studies have collectively suggested that the brain builds internal models of the body and environment in order to perform and predict the consequence of movements. However the temporal and spatial structure of these internal models have been subject of debate [5–8].

Here we focus on two recent models in motor adaptation. In temporal domain, the multi-rate model of adaptation, which was first proposed by [3], seems to explain the motor adaptation pattern in a class of perturbation environment called force-field. In this force-field environment human subjects hold a robotic manipulandum and make arm reaching movement while the robot applies a force to their hand. More recently, viscoelastic primitive model, developed by [5], associates force-field adaptation forces to the Newtonian kinematics of movements such as position and velocity and explains shape of force profiles within individual trials, thus suggests that structure for spatial pattern of motor adaptation is dependent on motion kinematics. Both models are described briefly here.

## 1.1 Multiple Rates of Motor Adaptation

Several motor adaptation studies, specifically force-field adaptation, have suggested the adaptation can be viewed as the output of a feed-forward state-space system with two internal states. The input to the state-space system is the error between the planned and executed motor output under the force-field. The states of the system, namely fast and slow, are separated according to their ability to learn from the error, and retain their previous state. The fast state responds to the error with a high gain, but has a weak memory of its previous state. The slow state on the other hand, responds to the error weakly, but the memory of the previous state is stable over many trials. These two states evolve independently, and the motor output is the combination of both states.

Many of the phenomena that are observed in motor adaptation experiments can be explained by the multi-rate model. For example, experiencing a force-field environment can create a memory that persists 24 hours after the initial exposure [4]. Interestingly, the amount of the memory on the second day depends on the number of force-field trials experienced on the first day and scales with the memory of the slow state of adaptation. Other phenomena including savings, spontaneous recovery, and anterograde interference have been investigated via the multi-rate model.

Although the multi-rate model of motor adaptation can give a meaningful picture about

the temporal evolution of the motor adaptation, it fails to capture the nuances in temporal shape of motor output within individual trials. The input, output, and states of the multi-rate model are one dimensional measures of motor adaptation, and are conventionally computed by performing a regression analysis between the subjects' applied force and the respective hand kinematic variable that is associated to the force-field. The output of the regression analysis is an adaptation coefficient that represents the similarity between the applied force and the ideal kinematic dependent force-field; adaptation coefficient of 0 and 1 defines no learning and complete learning of the environment, respectively. As a result, the multi-rate model limits the dimensionality of the forces applied by the subjects to one motion kinematic variable and ignores the Newtonian dynamics of the movements.

## 1.2 Viscoelastic Primitives for Motor Adaptation

Sing et al.[5] was the first group to propose an adaptation algorithm in force-field environments that is based on motion-dependent primitives, which we refer to as viscoelastic primitive model. This model is stemmed from extensive evidence for the representation of limb motion kinematics throughout the nervous system. In the viscoelastic primitive model, the motor output is represented as a weighted combination of primitives that are uniquely tuned to movement kinematics such as position and velocity. Similar to multi-rate model, the viscoelastic primitive model utilizes the error between the predicated and executed motor output to drive adaptation. However, the adaptation is mediated by the changes in the contribution from each primitive in the final motor output. The majority of the primitives are simultaneously dependent on both position and velocity of the movement, while few are tuned to only one of the kinematic parameter of the movement. When the motor system is experiencing a force-field that depends on only one kinematic variable, initial adaptation forces are consisted from both position and velocity of the movement. The model predicts that initial adaptation is dependent on a sub-population of primitives that have correlated tuning to both motion kinematics. As the adaptation progresses, the temporal shape of motor output becomes more aligned with the motion dependency of the force-field. Similar

behavior can be observed in the model, in which the weights for the primitives with correlated kinematic tuning are reduced while the weights for primitives that are appropriately tuned to force-field motion dependency gradually increase.

It is worthwhile noting that the learning in viscoelastic primitive model depends on the temporal shape of the motor response on individual force-field trials. Moreover, unlike the multi-rate model, the motor output is analyzed in two dimensions that are based on Newtonian mechanics of movements. As a result, this model captures the temporal changes in the motor output to a higher fidelity, when compared to multi-rate model.

Although the viscoelastic primitive model can be a good candidate model for motor adaptation to force-fields, it fails to capture the behavior of the motor system during unlearning of adaptation, as well as the retention of motor memory upon re-exposure. Here, we aimed build a model that can capture temporal characteristics of motor adaptation over many trials, and evolution of memory of these adaptation in the absence of perturbation in a unified manner.

Our approach was to combine the experimental analysis of motor behavior with state space models of motor adaptation. We specifically introduced populations of primitives with differential ability in learning from the error and retaining their memory. We divided our work in to 3 main parts; each included in a chapter in this thesis.

We first designed a series of experiments in chapter 2 in order to analyze the motor adaptations to force-fields that are uniquely tuned to the position and velocity parameters of movement. We further analyzed the unlearning of motor adaptation in these environments in order to capture both the time-scale and the motion dependencies in the motor adaptation memory.

We then introduced a model in chapter 3 that can reproduce the temporal details of motor adaptation within as well as between trials of the force-field environment. We extended current viscoelastic model in order to capture the behavior of motor system during unlearning period, where the prediction error is no longer available to the motor system. We showed that our model can predict the changes in the behavior of motor output between

adaptation and unlearning periods, as well as asymmetries in the motion-dependency of the adaptation.

In chapter 4, we focused on predictions that can be made by the new model when characteristics of force-field environment change. First we simulated the adaptation behavior in an environment where the force-field is introduced gradually. Next, we made predictions about the changes in the adaptation behavior if the force-field exposure extends over two days. We finally examined aspects of the motor adaptation that cannot be fully captured by our model and made an effort to set our future approach for extending generality of our model.

## Chapter 2:

### 2.1 Introduction

The motor system has an innate ability to adapt to imposing perturbations through experience. This adaptation is partly driven by the error between the predicted and executed movements on individual trials [9–13], and is associated with updating of an internal model that predicts the state of the body and environment [14–17]. In the absence of perturbation, the adaptation reverts back to its prior state. This reversion, which is referred to as unlearning, is a gradual process occurring over many trials and has been demonstrated in various motor adaptation paradigms, including prism adaptation [18,19], locomotion adaptation [20–23] and visuomotor adaptation [24–26]. The unlearning has also been studied in the force-field adaptation paradigm, where subjects are exposed to force patterns that are dependent on either a single limb motion kinematic, such as position and velocity, or their combination. In early studies of force-field adaptation the unlearning was prompted by simply removing the force-field perturbation, which resulted in an aftereffect in the movements that was in the opposite direction of the force-field and gradually disappeared [27]. However, the removal of the force-field does not equate to removal of error. Presence of aftereffects triggers feedback corrections of the movements as well as a new adaptation goal towards a non-perturbed environment, both of which mask the unlearning of the internal model [1,28–30].

To enhance earlier studies, error-clamp movement trials have been recently implemented to quantify the dynamics feed-forward of adaptation and unlearning to force-fields without activating feedback corrections [31–34]. Error-clamp movements are constrained to a straight path, which limits error based feedback corrections. Thus, the force that the subjects exert during these trials can reveal the details about dynamics of motor adaptation



and formation of internal models. The adaptation forces can be effectively reconstructed from a weighted combination of force states that are dependent on individual kinematic parameters of motion during these trials [5, 35–37]. Interestingly, early in adaptation, the forces contain similar weights from different motion-dependent force states. Extended exposure to the force-field increases the weight of the force state that is aligned with the motion dependency of the force-field, and decreases the force states that are misaligned. Although these studies have elucidated the evolution of motion-dependent force states and their contribution to the adaptation forces, they only explored the behavior of these force states in presence of motor error. The behavior of motion-dependent force states during unlearning of a force-field not been explored yet.

Here, we implemented novel force-field environments in order to study the unlearning of motor adaptation through the motion-dependent force state behavior. Our first hypothesis was that the evolution of these motion-dependent force states during unlearning would be distinct from adaptation given that the movement error was absent in the former. We tested unlearning in position-dependent and velocity-dependent force-field environments to explore this hypothesis. Further, we implemented two combination force-field environments in order to investigate whether there is any bias in the relationship between the imposing force-field and each of motion-dependent force state during both adaptation and unlearning.

## 2.2 Methods

### 2.2.1 Participants

Fifty six [(14,14,14,14) = (velocity FF, position FF, Combination FF, and Position-biased FF experiments)] healthy subjects without known neurological impairment were recruited from the George Mason University community to participate in the study. All participants were right-handed and performed the task using their right hand. Each individual participated in only one of the experiments. The study protocol was approved by the George Mason University Institutional Review Board, and all participants gave informed consent.

### 2.2.2 Experimental setup

The experimental setup was based on the standard force-field adaptation paradigm [14]. The subjects were instructed to move their hands to multiple targets in the sagittal axis of their body while grasping a robot manipulandum (Fig. 2.1). The manipulandum measured hand position, velocity, and force applied by the subjects, and its motors were used to apply forces to the hand, all at a sampling rate of 1000 Hz. In addition, a semi-transparent mirror was used to project the location of the hand and visual targets to the plane of movement while occluding the subject’s view of their hand (refresh rate of 60 Hz). During the experiment the subjects reached to circular targets 0.6 cm in diameter that were spaced 10 cm apart on the sagittal axis of the body.

The subjects were instructed to ”make quick reaching movements to the targets in both forward and backward directions”. At the end of each trial, the subjects received visual and auditory feedback about their movement. If their maximum movement velocity was between 0.25- 0.35 m/s and their movement time was shorter than 750 ms, the reach target (Fig. 2.1A) turned green and a beep sound played, indicating a good trial. Otherwise, if the movement speed was below 0.25 m/s, the reach target turned yellow with no beep sound, and finally, if movement speed was above 0.35 m/s, the reach target turned red also with no beep sound. The endpoint of each movement was used as the start point for the subsequent movement, and movements were made in two directions. the subjects received a performance score at the end of each block of movements, that indicated the percentage of good movements only in  $270^\circ$  direction; however, the subjects were unaware of this relationship and were only asked to maintain the score above 50% throughout the experiment. Only  $270^\circ$  movements with the maximum velocity between 0.2-0.4 m/s were used in the subsequent data analysis. In addition, the subjects had to initiate their movement within 75-2000 ms after the reach target appeared on the screen. Otherwise all targets were disappeared and the trial was immediately repeated.

Three trial types were used during the experiment: null, force-field, and error-clamp trials (Fig. 2.1B). Null trials were used for initial practice, where the motors of the robot

manipulandum did not apply any force to the hand. During force-field trials, the robot applied a force to the hand during  $270^\circ$  direction movements that was dependent either on movement position (with respect to start location), velocity, or a positive combination of position and velocity. The forces that the robot applied to the hand were always perpendicular to direction of movement, and had the general form shown in Eq. 2.1.

$$\begin{pmatrix} f_x \\ f_y \end{pmatrix} = c_K \times \begin{pmatrix} 0 & -K \\ K & 0 \end{pmatrix} \times \begin{pmatrix} x \\ y \end{pmatrix} + c_B \times \begin{pmatrix} 0 & -B \\ B & 0 \end{pmatrix} \times \begin{pmatrix} \dot{x} \\ \dot{y} \end{pmatrix} \quad (2.1)$$

In Eq. 2.1,  $K = 45N/m$  and  $B = 15Ns/m$ . For a position-dependent force-field (position-FF),  $c_K = \pm 1$  and  $c_B = 0$ , where  $c_K = +1$  and  $c_K = -1$  corresponded to clockwise and counterclockwise force fields, respectively ( the clockwise force-field is shown in Fig. 2.1B). For a velocity-dependent force-field (velocity-FF),  $c_K = 0$  and  $c_B = \pm 1$ , where  $c_B = +1$  and  $c_B = -1$  corresponded to clockwise and counterclockwise force-field directions. Combination force-field trials (Combination-FF) contained both position-dependent and velocity-dependent force-fields components, with  $c_K = \pm 1/\sqrt{2}$  and  $c_B = \pm 1/\sqrt{2}$  for clockwise and counterclockwise directions [5,35,36]. Lastly, Position-biased force-field trials contained both motion-dependent force components similar to combination FF, However the contribution of position-dependent component was greater, with  $c_K = \pm 0.849$  and  $c_B = \pm 0.528$ . Each subject experienced only one type of force-field throughout the experimental session. Finally, during error-clamp trials, the robot motors constrained movements in a straight line toward the reach target by counteracting any motion perpendicular to the target direction [4,38]. This was achieved by applying a stiff one-dimensional spring ( $6kN/m$ ) and a damper ( $150Ns/m$ ) in the perpendicular axis to the reach direction. In these trials, perpendicular displacement from the straight line to the reach target was held to less than 0.6 mm and averaged about 0.2 mm in magnitude.

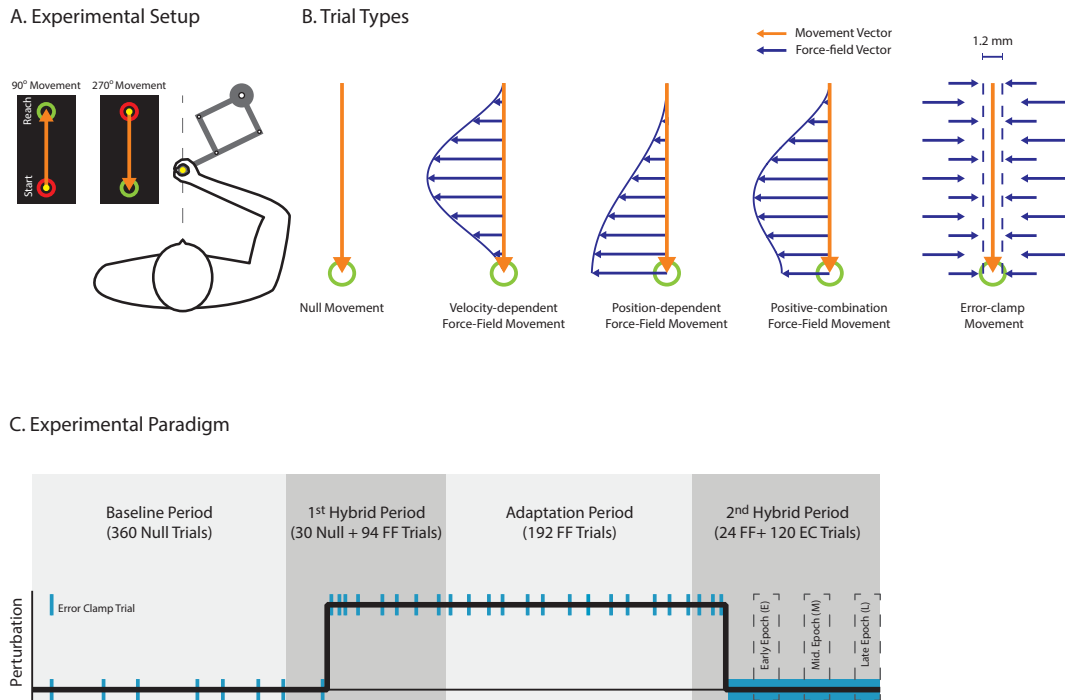


Figure 2.1: Subject made reaching movement in mid-line of their body in both forward  $90^\circ$  and backward  $270^\circ$  directions, using a robotic. (A) The spatial location of their hand was reflected to its perspective location on the screen (yellow circle), while the view of arm was occluded. (B) Trial Types: Null movements (orange arrow) were made in the absence of the any force from the robot. During force-field trials movement, the robot applied forces that were dependent on a single of combination of motion kinematics. Velocity-dependent force-field movements were made in the presence of a lateral force that was scaled with hand velocity (blue arrows). For position-dependent force-field movements, the lateral force was scaled with the hand position with respect to the start point of movement. Lastly, for both combination and position biased force-field movements, the force scaled with both hand position and velocity. During error-clamp movements were channeled in the direction of reach target (dashed lines) by implementing a virtual spring damper system that opposed any lateral motions. (C) Experimental Paradigm: Subjects first completed a baseline period, during which they experienced null movement with sparse instances of error-clamp movements (blue bars). 1st hybrid period, contained initial period of null movements that followed by force-field movements. The frequency of error clamp trials was increased during force-field trials. Adaptation period contained only force-field and error-clamp trials. Finally the 2nd hybrid period started with 24 force-field movements, which then followed by only error-clamp trials (thick blue bar). The sequence of error-clamp trials signified unlearning period after adaptation, and contained early, mid, and late epochs.

### 2.2.3 Task

To observe both the force-field adaptation and unlearning behaviors, each subject experienced the experimental paradigm shown in (Fig. 2.1C). Subjects performed sets of  $90^\circ$  and  $270^\circ$  movements; however all  $90^\circ$  movements were made under error-clamp condition, and the force-field was only applied to  $270^\circ$  movements, and only the  $270^\circ$  movements were used for analysis of adaptation and unlearning. Subjects also experienced random error-clamp trials in  $270^\circ$  movements during baseline and adaptation periods. During unlearning period, however, they only experienced error-clamp trials in both directions.

Each experiment started with a baseline period, where subjects completed 360 null trials. These null trials were divided into 4 blocks. During this period, 12 error-clamp trials in were pseudo-randomly interspersed between  $270^\circ$  movements, In order to measure the baseline levels of forces for each subject. The average lateral force during these trials were then subtracted from the error-clamp trial forces in adaptation and unlearning periods.

Following the baseline period, subjects experienced the 1st hybrid period, during which the force-field environment was introduced after an initial 30 null trials. We designed the 1st hybrid period to capture the immediate changes in subject forces due to experiencing the force-field for the first time. The 1st hybrid period was followed by 2 blocks of adaptation in which the subjects experienced only one of the force-field environments, i.e velocity-FF, position-FF, Combination-FF, or Position-biased-FF. Similar to the baseline period, here we pseudo-randomly inserted 26 error-clamp trials in  $270^\circ$  direction in order to measure the adaptation level at different points. The sign (direction) of the FF remained constant for each subject, but counterbalanced between subjects. In other words, the first group of six subjects experienced the force-field in counterclockwise direction and the second group of six subjects experienced the force-field in clockwise direction. Finally, after the adaptation period, subjects experienced the 2nd hybrid block. This block started with 24 force-field trials, and followed by 60 consecutive error-clamp trials. We refer to these 60 error-clamp trials as unlearning period, during which the adaptation returns to baseline level prior to experiencing the force-field. Inclusion of the unlearning period within the hybrid block

effectively masked any context dependent changes in the behavior of the subject due to the removal of force-fields [8].

#### 2.2.4 Analysis of Force Profiles

Previous force-field adaptation studies have suggested that adaptation involves two processes, first, a predictive adaptive process that compensates for the expected force in the upcoming movement, and a second online feedback process which corrects for the error experienced during the movement [1,28,30]. The implementation of error-clamp trial eliminated any lateral errors in movement that might trigger online feedback corrections. Given that the lateral force during error-clamp trial reflected the predictive adaptive responses to the force-fields, we limited our analysis to these forces. Based on Eq. 2.1, subjects could fully compensate the force-field only when they produce a force that was proportional to their movement velocity, position, or their positive combination and opposite to the direction of force-field. With this knowledge, we first computed the ideal force by implementing subject’s longitudinal movement kinematics (position, velocity) during the error-clamp trial in Eq. 2.1. The movement and force profiles were truncated with a temporal window of 1500 ms centered at the peak velocity. We made sure this temporal window include the complete progression of each movement. Next we defined an adaptation coefficient by performing a linear regression between the ideal force and the lateral force applied by subjects during the same error-clamp trial [4,38–40]. We computed the adaptation coefficient for each subject during both adaptation and unlearning periods and averaged the values over all subjects.

We further characterized adaptation and unlearning behavior by projecting the lateral force during each error-clamp trial onto a two dimensional space that parsed position dependent and velocity dependent components of force. We refer to this 2-dimensional space as gain-space of learning [5]. The gain space represents complete adaptation to a velocity-dependent force-field by point  $[0, 1]$ , position-dependent force-field by point  $[1, 0]$ , combination force-field by point  $[1/\sqrt{2}, 1/\sqrt{2}]$ , and finally a position-biased force-field by point  $[0.849, 0.528]$ . Moreover, the x and y parts for each point in this space correspond to

adaptation of position-dependent and velocity-dependent components, respectively. In order to delineate adaptation in gain-space, we first calculated a multiple regression between the lateral force during the error-clamp, and both position and velocity of movement. We then rescaled the coefficients for position and velocity components by 45 N/m and 15 Ns/m factors, respectively, and projected them to the gain-space. We performed this analysis for each subject calculated the average gains over all subjects [5, 35–37].

In order to capture the temporal changes of adaptation level during unlearning, we operationally defined three epochs of unlearning during 2nd hybrid period (Fig. 2.1). Early, middle, and late unlearning epochs were defined as first, third, and last 10 error-clamp trials in  $270^\circ$  direction after the start of unlearning period, respectively. Two-paired one-sided and two-sided student t-tests were performed between different force-field groups to compare the unlearning behavior at each epoch. We further performed two-way ANOVA to compare the effect of different force-field type, and epochs on the unlearning behavior of the subjects.

## 2.3 Results

We designed series of experiments to characterize the dependency of unlearning to motion states after adaptation to a novel force-field environment. We specifically looked at the temporal differences in exerted force profiles during unlearning when subjects previously had adapted to pure position or velocity-dependent force-fields. We then introduced a new group of subjects to two new combination force-field in order to modulate the asymmetries we observed between unlearning of pure position and velocity-dependent force-fields.

### 2.3.1 Adaptive Responses to a Position- and Velocity-Dependent Force-field

We trained 14 subjects in the position-FF and another 14 subjects in the velocity-FF environment. Each subject experienced only one type of force-field after an initial baseline period. Previous studies have shown that subjects can adapt to both type of force-fields

and achieve asymptotic levels after 140-200 trials [3–5, 14]. We similarly observed an initial fast progression of adaptation which plateaued after 120-150 trials for both force-fields (Fig. 2.2). Early adaptation was faster for the position-dependent force-field. However, as learning progressed the difference between velocity FF and position FF adaptation dropped below significance.

Immediately after adaptation period, subjects experienced a sequence of consecutive error-clamp trials, which identified as the unlearning period. With initiation of unlearning period, the adaptation coefficient started to decay immediately and reached an asymptotic level by the end of the period. Previous studies have similarly shown that subjects monotonically decrease the exerted force in the absence of error [32, 34]. Even though the patterns of unlearning were similar for both position FF and velocity FFs (Fig. 2.2), we further analyzed their differences acknowledging that final adaptation levels were slightly different between the two cases. In order to balance the unlearning with respect to the final adaptation levels, we divided the adaptation coefficients during unlearning by the initial value of the period, thus the first point of unlearning is scaled to 1 (Fig. 2.2B). We then analyzed the unlearning in three epochs, i.e. early, mid, and late (E, M, and L). In both early and middle epochs, unlearning of position FF and velocity FF are similar ( $p > 0.05$ ), however, late epoch the velocity-FF adaptation coefficient is higher ( $p < 0.05$ ). This result was surprising; we thus performed a 2 way ANOVA to investigate whether the type of force-field had a significant effect on unlearning. As expected, the type of force-field had no significant effect on the unlearning pattern (2 way ANOVA,  $p=0.28$  for the main effect of force-field type, and  $p < 0.05$  for the main effect of epoch, and  $p < 0.05$  for the interaction).

Although the one dimensional measure adaptation coefficient showed stereotypical behavior during adaptation and unlearning of velocity-FF and position-FF, previous studies have demonstrated that the temporal characteristics of learned force profiles cannot be fully captured by this measure [5, 35, 37]. Therefore, we compared the temporal shape force profiles with position and velocity of motion states in early and late phase of the adaptation as well as unlearning. Early in the adaptation period the force was dependent on both velocity



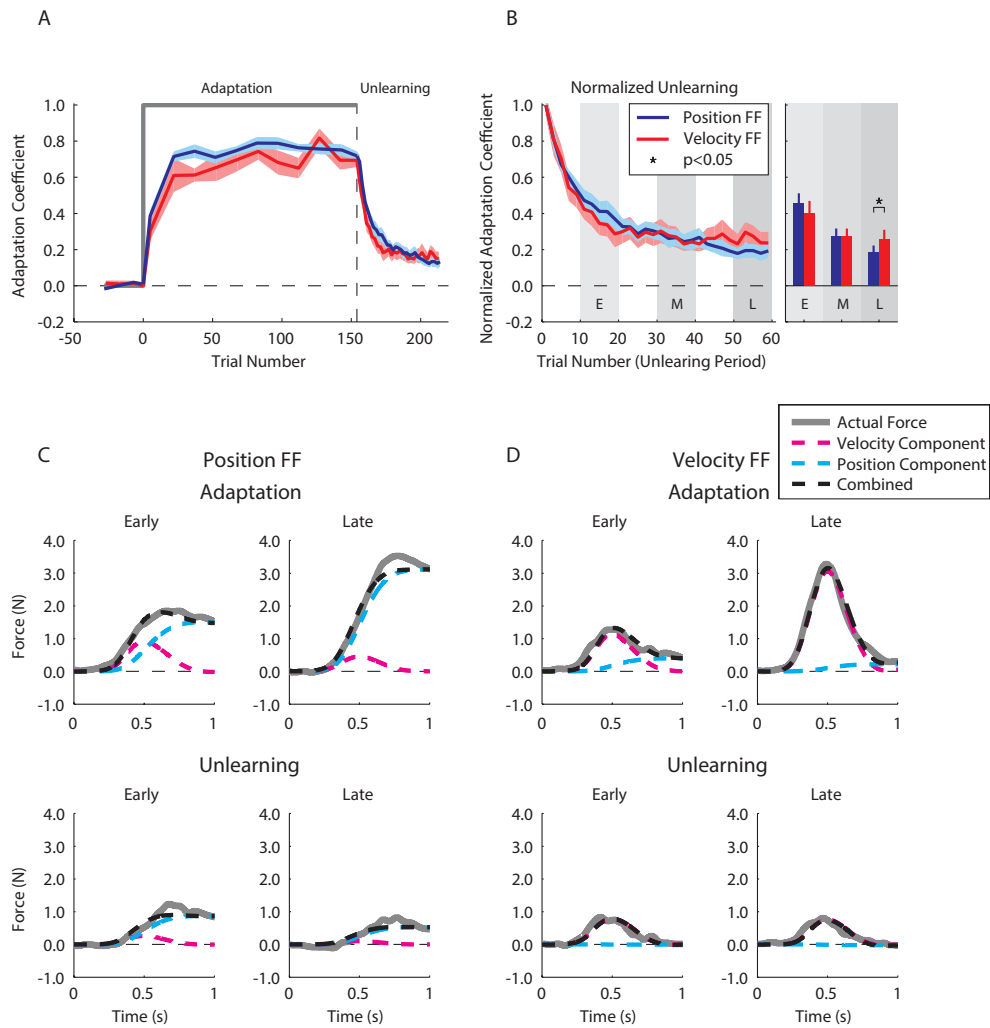


Figure 2.2: Comparison between adaptation coefficients for the position-FF (blue curve) and velocity-FF (red curve) groups. (A) Each point during adaptation period is the average adaptation across all subjects for a window of 15 trials. During unlearning period, the points were average across subjects for a window of 2 trials. The start of unlearning period is shown with a vertical dashed line. Shaded areas show S.E. (B) Normalized unlearning for the position-FF and velocity FF groups were calculated by scaling adaptation coefficients with respect to the first point in the period. Thus the first point is rescaled to 1. Bar graphs show the average adaptation across subjects for early, mid and late epochs of unlearning, which represented by the shaded areas. Error bars are S.E. (C,D) Temporal profile of the forces during adaptation and unlearning of Position-FF and Velocity-FF. Top panel shows evolution of the force in early and late stages of adaptation, while the bottom panel shows the changes in early and late stages of unlearning period. The average force across all subjects is shown by a gray curve. Position and velocity-dependent force states are shown by blue and pink dashed lines, respectively, and were calculated by performing a multiple regression between the force, position, and velocity of the movements. The combination of position and velocity force-states is shown by a black dashed line, and approximates actual exerted forces.

and position of the movement, whereas late in the adaptation, the force is mostly aligned with the appropriate movement parameter for the force-field adaptation. In other words, the force exerted by the subjects in late phase of a position-FF adaptation was aligned with position state of the movement, and in late phase of velocity-FF adaptation was aligned with velocity state of the movement, both are consistent with previous observations [5].

Unlike adaptation period, movements during unlearning period were channeled and any lateral errors were precluded entirely by the error-clamps. The absence of error can affect the force profiles differently compared to the adaptation period. We therefore analyzed the force profiles in early and late phase of unlearning. Interestingly, the force profiles remained aligned to the appropriate motion state for experienced force-field in both early and late stages of unlearning (bottom panels in Fig. 2.2). In early phase of unlearning for the position-FF, the force profiles mainly consisted of a position-dependent component, and the velocity dependent component is minimal. In late phase, the position-dependent component remained to contribute to most of the exerted force and the velocity component was almost at zero (Fig.2.2C bottom panel). Similarly, force profiles in both early and late phases of the velocity-FF unlearning were mostly consisted of velocity-dependent component and position dependent component did not return to its previous level during the adaptation period (Fig. 2.2D). When we observed the dissociation in the expression of motion-dependent force components between adaptation and unlearning periods, we decided to further delineate how the motion-dependent force components evolve during each period in the gain space of learning.

### **2.3.2 Gain-Space Analysis of Adaptive Responses to Single State Force-fields**

When we analyzed the force profiles for the adaptation and unlearning periods in the two dimensional gain-space and parsed the position-dependent and velocity-dependent force components, we found a clear separation between adaptation and unlearning trajectories for both position-FF and velocity-FF (Fig. 2.3A and B). For both type of force-fields, we

identified a goal aligned and a goal misaligned component. The goal aligned component for position-FF is parallel to x-axis in the gain-space and represents position-dependent force component, whereas the goal misaligned component is parallel to the y-axis in gain-space and represents velocity-dependent force component. On the other hand, for the velocity-FF, the goal aligned and goal misaligned components represent velocity and position-dependent force components, respectively.

In Both the velocity-FF and position-FF, initial adaptation was mediated by the contribution of both goal aligned and goal misaligned force components with similar degrees. As the subjects experienced the force-field, the contribution of the goal aligned component increased whereas the goal misaligned component decreased (Fig. 2.3A and B). By the end of adaptation period the force were consisted mostly from the goal aligned force component. This was more evident when we looked at the location of the gains by the end of adaptation. Late adaptation position-FF gains were close to the x-axis, which represents pure position-dependent forces. Similarly, late adaptation velocity-FF gains were close to the y-axis, which indicates pure velocity-dependent forces [5].

The gains started to diverge from previous adaptation trajectory with the start of the unlearning period ( gray lines in Fig.2.3A and B). In both force-fields the direction of change in gains was toward the origin of the space; however the gains never returned completely to the origin, which indicates partial unlearning of the force-fields. This is corollary to the asymptotic behavior in unlearning adaptation coefficient that we observed previously. The separation of the adaptation and unlearning gains in both position-FF and velocity-FF demonstrates a hysteresis in the behavior of motor system during unlearning of the adapted force-field. This can be a direct effect of the presence or absence of error during individual movements.

We particularly were interested in investigating the temporal changes in the gain of goal misaligned component given that the hysteresis is a direct result of its behavior. Fig. 2.3C shows the gains for both aligned and misaligned components for position FF during adaptation and the following unlearning period. In order to capture the changes in goal

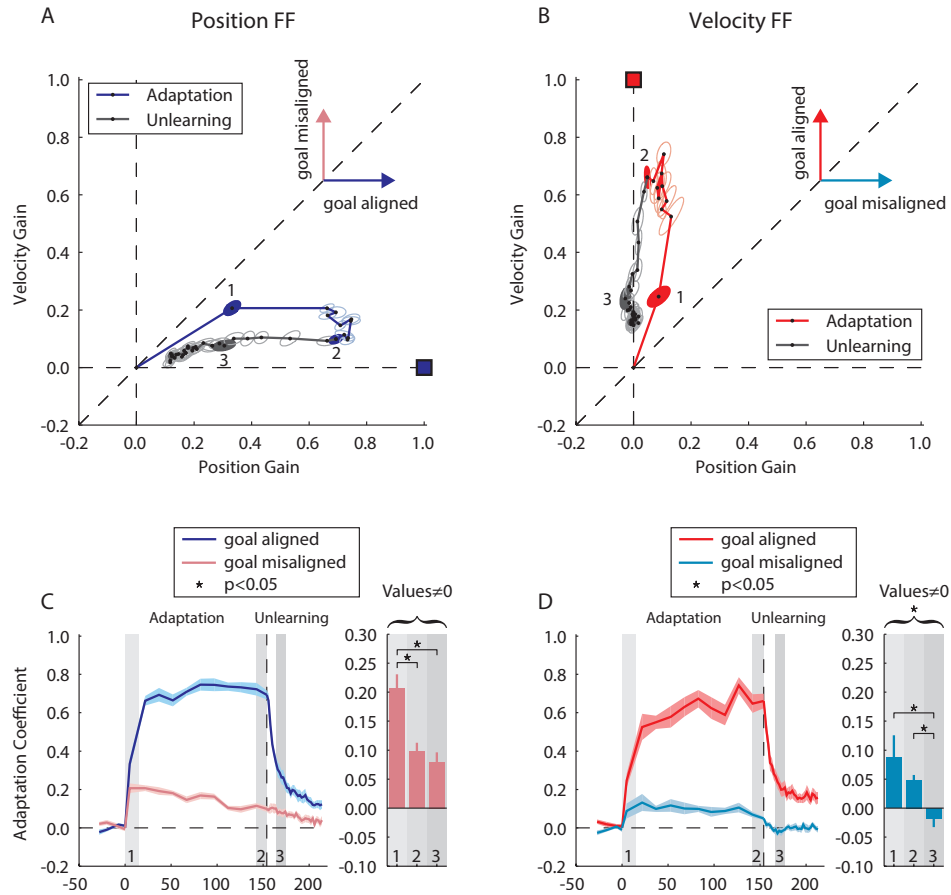


Figure 2.3: (A) Evolution of position and velocity gains during adaptation and unlearning of the Position-FF. Gain trajectories during adaptation and unlearning periods are shown in blue and gray, respectively, and are averaged across all subjects. The adaptation goal is shown as a blue filled square. Each gain can be broken down into goal-aligned and goal misaligned components, as shown by two vectors. Ellipses show standard error for subjects. 3 points are selected for further comparison of goal misaligned gains, shown as filled ellipses and also by numbers 1, 2, and 3. (B) Evolution of position and velocity gains during adaptation and unlearning of a velocity-FF. Adaptation gains are shown in red, and unlearning gains in gray. Goal of adaptation is represented by a red square. Here direction of the goal aligned and goal misaligned components of each gain are shown by a red and cyan arrow, respectively. (C,D) The temporal changes for goal-aligned and goal-misaligned components are shown for each force field environment, shaded area shows the standard error values. Bar graphs show the amplitude of goal misaligned component for the point that are highlighted in part A, and B as 1, 2, and 3. Error bars show standard error of gains for each point.

misaligned component, we picked 3 points in gain space, 1st and 2nd points were during early and late adaptation, and the 3rd point was during unlearning period. Importantly, 1st point and 3rd points had the same goal aligned component amplitude. This was done on the premise that the difference in the amplitude of goal misaligned component between 1st and 3rd points signifies the separation between adaptation and unlearning gains, thus demonstrates the hysteresis.

For the position-FF, the value of goal misaligned component at the 1st point was different from both 2nd and 3rd points (Fig. 2.3C). The difference between the 1st and 2nd points showed that the early adaptation level was less specific to the force-field compared to the late adaptation. The difference between the 1st and 3rd points further showed that for similar values of goal aligned component, adaptation and unlearning gains were separated. The goal misaligned component was always different from zero for all 3 cases, so both adaptation and unlearning were confined in the 1st quadrant of the gain-space. The behavior of goal misaligned component was slightly different for the velocity-FF, but the overall effect was the same. Here, the goal misaligned component value changed from 1st point adaptation to the 3rd point in the unlearning, again showing that the trajectories were different between the two periods. The position-dependent component values for early and late adaptation were not different, which might be surprising. We can expect this result if we take to account that the gains for velocity-FF are more aligned to the goal compared to position-FF. We also observed that gain trajectory entered the 2nd quadrant for the 3rd point in the velocity-FF unlearning, and was no longer confined to first quadrant of space. However when we analyzed the gains for late unlearning we did not observe this effect any more.

Although the hysteresis was present in both velocity and position FFs gain trajectories, the shapes of trajectories were not completely similar. We identified two sources of asymmetries between gain space trajectories. First, during the adaptation period the initial learning were less specific for position-FF compared to velocity-FF. This caused the velocity-FF adaptation gains to be more aligned with the goal compared to position-FF. Second, there was more curvature in the unlearning gain trajectory for position-FF and

further it was confined in the 1st quadrant, whereas the unlearning gain trajectory for velocity-FF aligned with the goal (y-axis) and had less curvature. We hypothesized that these asymmetries were due to intrinsic bias in the subjects' ability to associate the imposing force-field with kinematics of their movements and are not merely due to noise. If the association between movement kinematics and force-field was skewed toward the velocity of the movement, then adaptation to a new force-field which is equally dependent to position and velocity should be skewed toward velocity as well. This effect should maintain during unlearning of the force-fields as well. Thus we trained two new groups of people in novel combination force-fields to test this hypothesis and further characterize the asymmetries that we observed.

### 2.3.3 Gain-Space Analysis of Combination Force-Field

We introduced a new group of 14 subjects to a combination force-field with equal contribution from position and velocity of the movement in order to further characterize the asymmetries we observed between that gain trajectories of position and velocity-FFs. Previous studies have shown that adaptation to combination force-field is generally faster than a pure position or velocity-dependent force-fields [5, 36]. Here we examined the ratio between the position and velocity-dependent force components during both adaptation and unlearning periods.

We observed that the adaptation level was generally closer to the goal by the end of the adaptation period in the combination-FF. Subjects initially adapted to the force-field using similar gains for position and velocity, however, by the end of adaptation period, the velocity-dependent gain contribution became greater than the position-dependent gain, which caused the adaptation gain trajectory to be tilted towards the velocity gain axis (y-axis in Fig. 2.4A). With the start of unlearning period, the gain trajectory started to decay toward origin of the space, however the velocity gain remained higher than the position gain throughout the unlearning period (Fig. 2.4A, gray line).

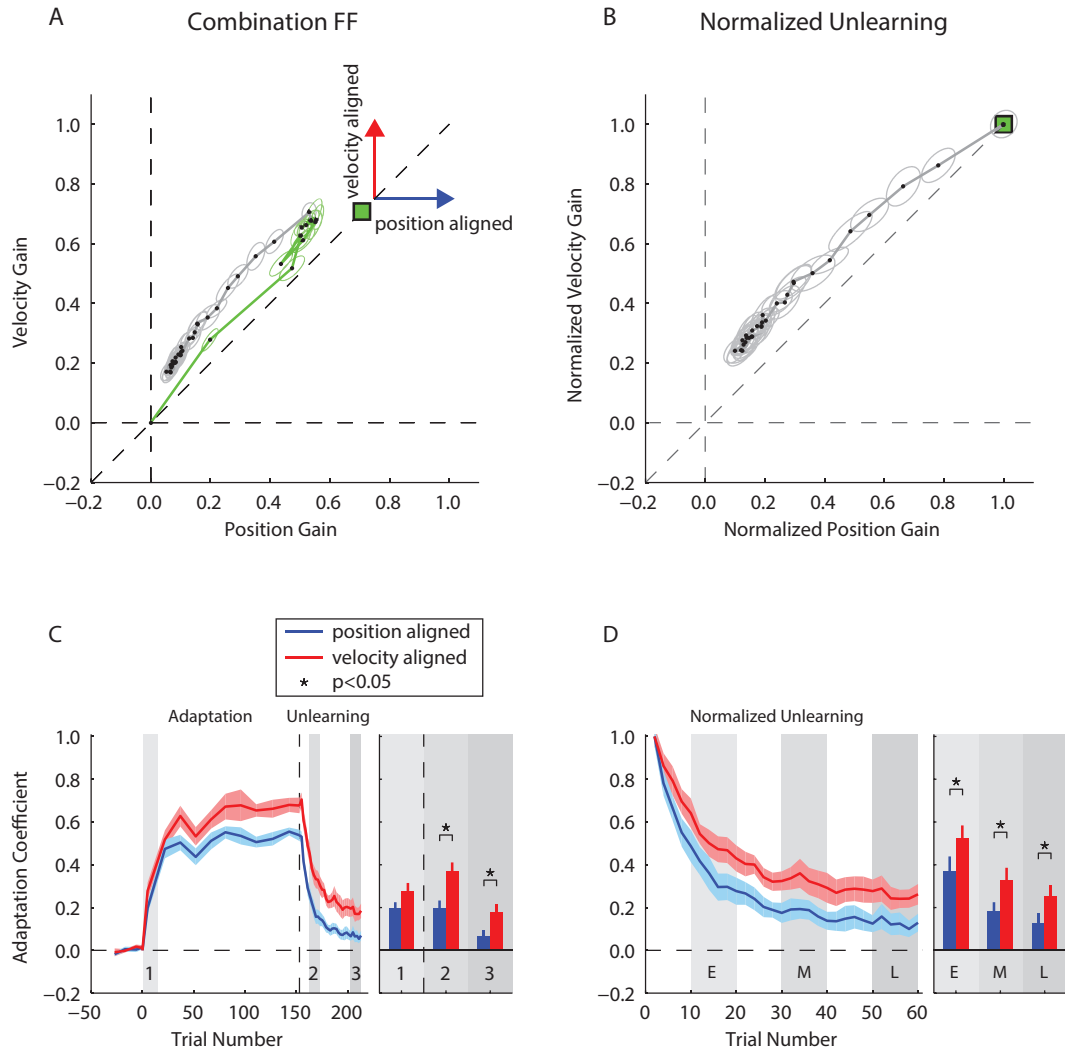


Figure 2.4: (A) Adaptation gains are shown with green solid line, whereas unlearning gains are shown in gray. Here the goal of adaptation is shown by a green square and located on  $x = y$  line. The directions of position-aligned and velocity-aligned components are shown by blue and red arrow respectively. (B) The normalized unlearning gains were computed by rescaling the gains during unlearning by their respective starting points, thus the first point is rescaled to [1,1] in gain space. The gray line represents the normalized unlearning, and the ellipses shows standard error at each point. (C) Temporal changes in position-aligned and velocity-aligned gains during adaptation and unlearning of the combination force-field. The position aligned gains are shown in blue and the velocity-aligned gains are shown in red. The bar graphs show the amplitude of each component for the shaded region numbered in the left panel. (D) Normalized unlearning of position and velocity aligned gains. The bar graph depicts the comparison between normalized gains in early (E), middle (M), and late (L) epochs Error bars show standard error of gains for each epoch.

We further examined the temporal changes of gains during both adaptation and unlearning periods by projecting the gain trajectory onto the position and velocity axes at each point (Fig. 2.4C). Early in adaptation the position and velocity gains had similar amplitudes, however, the velocity gains became significantly greater than the position gain by the end of the adaptation period. This significant difference between the velocity and position gains extended to the unlearning period (Fig. 2.4C, 2nd and 3rd bar graphs). This clearly shows that when the force-field is equally dependent on the position and velocity parameters, the velocity-dependent force component contributes more than position-dependent force component during both the adaptation and unlearning periods. This correlates with the asymmetry between the velocity-FF and position-FF gain trajectories that we observed previously and suggests that bias in toward velocity-dependent force component might be an intrinsic property of motor system when adapting to force-fields and it is not merely an effect of noise.

If the shape unlearning trajectory in Fig. 2.4A was a result of unequal learning at the end of adaptation, then the normalized unlearning should be aligned with  $x = y$  line in gain space. However, the result clearly contradicts this assumption (Fig. 2.4B). The velocity gain contribution was always greater than position throughout the normalized unlearning. When we looked at the temporal changes of the normalized gains for unlearning, we observed the same effect (Fig. 2.4D). Specifically for early, mid and late epochs of unlearning, the normalized velocity gain was greater than that of position.

We wondered whether the bias that we observed in combination-FF is local for the velocity dominant gains. As a result we run the 4th group of subjects in a combination force-field which was biased toward the position-dependent component. The adaptation gains for this field were biased towards the position dominant gains as seen in Fig. 2.5, and the adaptation trajectory lied in the portion of gain-space with higher position gains. However with the start of the unlearning period gain trajectory diverged toward the velocity dominant gains and lied completely in that region by the end of unlearning. This can be seen in the temporal changes of both gains during adaptation and unlearning period



(Fig.2.5C). Even though the adaptation started with equal contribution from both gains, late adaptation was clearly dominated by position gain. With the start of unlearning there is a sudden drop in the position-dependent gain, while the decay of velocity-dependent gain is slower, which resulted dominance of velocity-dependent gains over position-dependent gains during unlearning.

We also looked at the normalized unlearning of the position-biased force-field and observed that the normalized unlearning was pulled towards the velocity axis. This effect was strongly present in all epochs of unlearning(Fig. 2.5B, and D).

These results clearly support our hypothesis that there can be a bias in the association between the force-field and position and velocity of movements, and this bias is towards the velocity of movement. The bias seems to be present during both adaptation and unlearning periods, further suggesting that the force-field does not necessarily enforce the bias, instead the motor system plays a role in the causing the bias.

### **2.3.4 Comparison of Unlearning Behavior Between Different Force-field Environments**

Given the asymmetric behavior during the unlearning periods, we wondered whether the timescale of unlearning for each motion dependent force states is tied to its spatial location in gain space during adaptation. In other words, we asked whether the stability of each motion-dependent memory is modulated by the force-field. In Fig. 2.4 we showed that even when the force-field goal has equal contribution from velocity and position of movement, both adaptation and unlearning are biased toward the velocity component suggesting that the velocity component is more stable than the position. As a result, we examined the unlearning of position-dependent components between position-FF and two combination-FFs, and similarly velocity dependent components between velocity-FF and combination-FFs (Fig. 2.6).

The position dependent force-state was most stable during unlearning of pure position-dependent force-field (Fig. 2.6B), even in case the unlearning trajectories are normalized

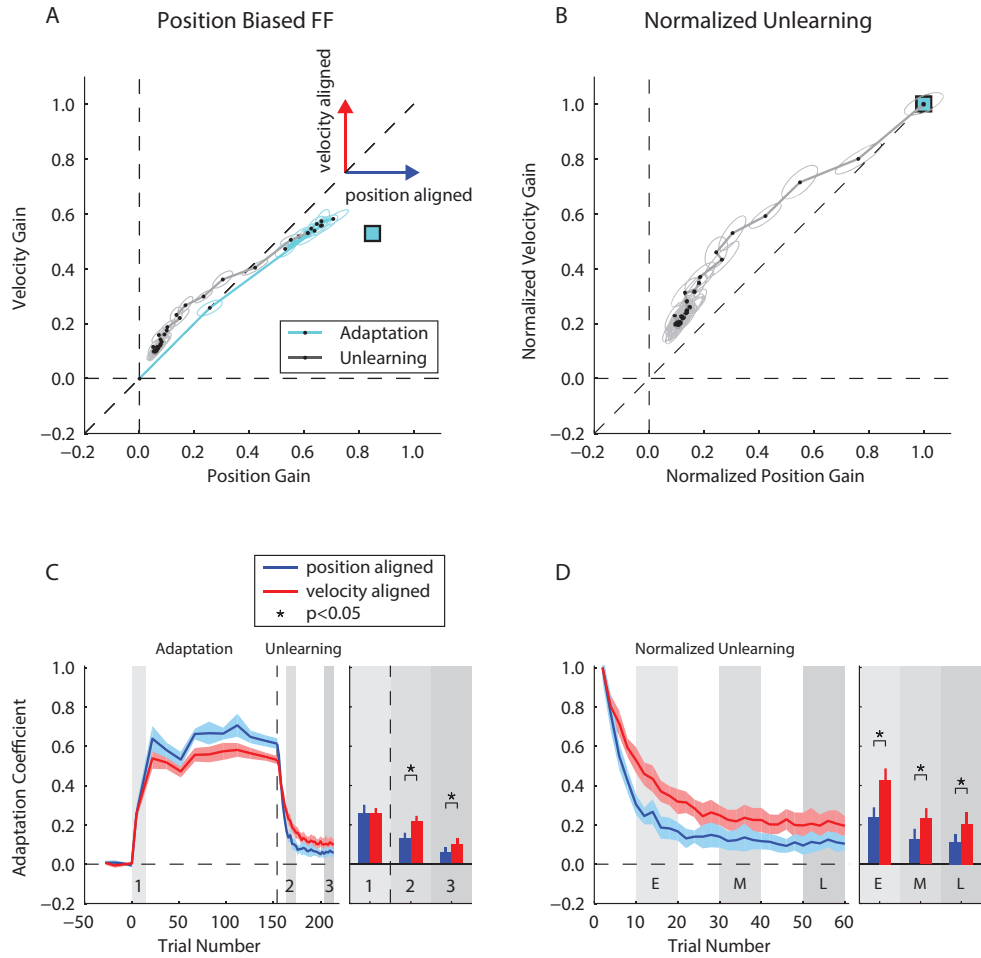


Figure 2.5: (A) Adaptation gains are shown with cyan solid line, whereas unlearning gains are shown in gray. Here the goal of adaptation is shown by a filled cyan square and located in a region of gain space with larger position gain than velocity. For each gain the direction of position aligned and velocity aligned components are shown by blue and red arrow respectively. (B) The normalized unlearning gains were computed by rescaling the gains by their respective start points value, and the unlearning starts from point [1,1] in gain space. The gray line represents the normalized unlearning of gains, and the ellipses show standard error for each point. (C) Temporal changes in position-aligned and velocity-aligned gains during adaptation and unlearning of the position-biased force-field. Position aligned gains are shown in blue and velocity-aligned gains are shown in red. The bar graph shows the comparison between position-aligned and velocity-aligned gains at the points selected in left panel. (D) Normalized unlearning of position and velocity aligned gains. Three epochs of unlearning are shaded. The bar graph depicts the comparison between normalized gains in early (E), middle (M), and late (L) epochs. Error bars show standard error of gains for each epoch.

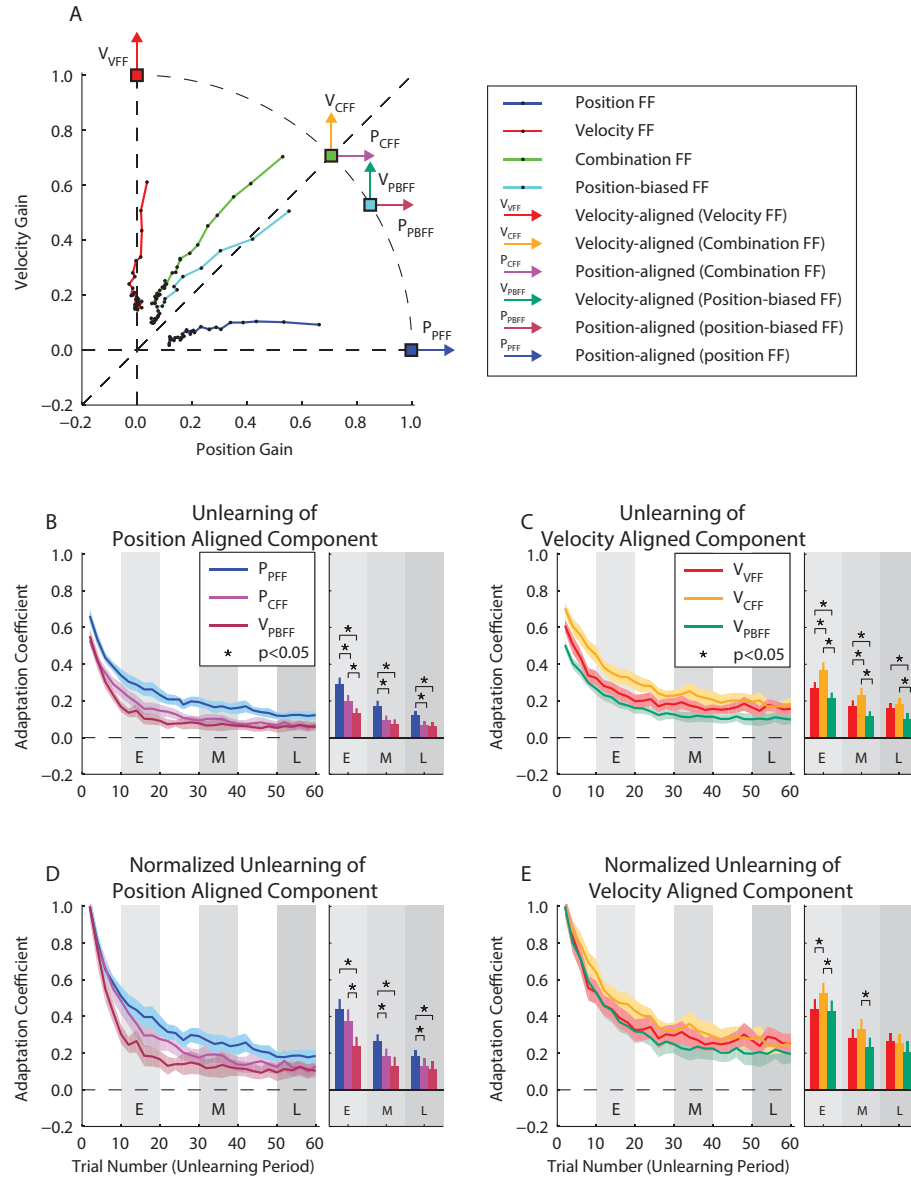


Figure 2.6: (A) gain space representation of decay of motor memory after each force-field adaptation. For each force-field a position-aligned and a velocity aligned vector identified during unlearning. (B) Unlearning of position-aligned component for position-dependent, combination, and position-biased force-fields. The bar graphs compare the strength of the position-aligned component after each force-field in three epochs of unlearning. (C) Unlearning of velocity-aligned component for velocity-dependent, combination, and position-biased force-fields. The bar graphs compare the strength of velocity-aligned component after each force-field in three epochs of unlearning. (D,E) Normalized unlearning of the position and velocity aligned components in the force-fields shown in B and C, respectively. Three epochs of unlearning are shaded. The bar graphs depict the comparison between normalized gains in early (E), middle (M), and late (L) epochs. Error bars show standard error of gains in each epoch.

against their initial value (Fig. 2.6D). Interestingly, the position-dependent force state was less stable when it was learned in the combination-FF. This might suggest that stable position-dependent force-states are aligned along the position-gain axis, and are mostly excited in a pure position-FF environment.

On the other hand, Initial inspection of velocity-dependent force-state unlearning suggested that combination-FF with equal contribution of both states as well as velocity-FF has the most stable memories (Fig. 2.6C). However when we normalized the unlearning trajectories, this relationship did not hold anymore and the velocity-dependent force-state for velocity-FF, position-biased-FF, and combination-FF exhibited similar decays (Fig. 2.6E). The velocity-dependent component in the combination-FF unlearning remained to be more stable early epoch, but in late epoch this difference dropped below significance and velocity dependent force state for all force-fields became similar. One possible explanation for this behavior might be that the adaptation is strongest for the equal-combination-FF, compared to the other two cases, which might trigger more stable component of memory in late stages of adaptation. Nonetheless, the similarity between different velocity-dependent force-states suggests that there is a greater distribution of stable velocity-dependent force-states throughout the gain space which manifested in similar rate of unlearning independent of ratio between position to velocity dependency imposed by the force-field (Fig. 2.6A and E).

## 2.4 Discussion

We investigated the evolution of motion-dependent force-states during adaptation and unlearning of position- and velocity-dependent force-field environments, and observed a clear hysteresis between the trajectories of adaptation and unlearning. This hysteresis is a direct effect of the decrease in the contribution of goal misaligned force-state in unlearning compared to adaptation. In single field data, hysteresis effect is smaller for velocity-FF compared to position-FF. This observation was further investigated in the unlearning trajectories for two combination force-field environments in which the external perturbation

depended on both the position and velocity of the movement. The velocity-dependent force-state tended to be more stable during the unlearning of the combination force-fields, which resulted in a bias toward velocity axis in the gain trajectories of unlearning .

#### 2.4.1 Previous Studies of Unlearning of Motor Memory

Unlearning of motor memories has been previously studied in different contexts including visuomotor and force field adaptation. In visuomotor adaptation tasks, unlearning can be induced by removal of visual feedback of the hand location, visual error clamps, removal of rotation, or simply passage of time[26]. However, the gradual unlearning towards the baseline performance occurs only when the motor system is actively engaged in the task. This engagement in the task is thought to continually modify the internal model of the body and environment in cerebellum.

Similar to visuomotor adaptation task, force-field adaptation studies have demonstrated unlearning by utilizing error-clamp trials, null trial, or passage of time. The unlearning due to error-clamp trial has been linked to fast and slow components which can learn for the error, but their ability to retain the adaptation is different. A recent study has put forward the idea that the unlearning provoked by error clamp trials is a stochastic process that is dependent on the subjects' knowledge about the changes in the environment [8]. Our current results, however, contrasts this idea. We observed that the unlearning was triggered by the removal of the error, even though the pattern of unlearning is dependent on the nature of learned environment. Recent observation by other labs have also shown that the unlearning is dependent on prediction errors [41].

Other mechanisms might be responsible for our observation of specificity of unlearning. Ingram et al.[42] previously have demonstrated that the rate of experience-dependent unlearning is regulated by the spatial overlap between the adaptation movements and the following error-clamp movements. The unlearning was maximal when both performed in the same spatial location and orientation. Their observation can be viewed with respect to primitives that are spatially tuned to the task. We instead quantified adaptation based

on primitives that were tuned to different motion kinematics with varying gains. By the end of adaptation period, the motor adaptation memory was built from the primitives that were closely tuned to adaptation goal. Experiencing a sequence of error free movements during unlearning period attenuated the memory of the tuned primitives but does not evoke memory of primitives that were inappropriate for the task.

#### **2.4.2 Neural Correlates of Motion-dependent States in Motor System**

The idea of motion-state dependency in the adaptive motor response has been supported by several neurophysiological studies that have examined the correlation between patterns of neural activity and motion state variables. For example, the simple spike activity of Purkinje cells in the primate ventral paraflocculus during an ocular following response can be approximated as a linear combination of the acceleration, velocity and position changes during the eye movement [43]. Similarly, during a saccadic adaptation task, complex spike activity of Purkinje cells located in the vermis of the oculomotor cerebellum are tuned to the direction of eye movement position errors - neural signals that may drive and modulate the subsequent adaptive responses [44].

There is evidence for a representation of limb motion kinematics as well as kinematic errors in the neural responses of Cerebellar Purkinje cells [45–48]. Similarly, the firing rate of Neurons in primary motor cortex correlates with the kinematics variables of limb movement including direction [49], position and velocity [50,51], as well as forces associated with the limb movement [52]. One study in particular showed that in visual tracking movements, firing rate of neurons had a sinusoidal turning to both position and velocity of the movement and scaled linearly with distance and speed [51]. The tuning of the neural activity to the position and velocity has also been shown in human motor cortex [53]. On the other hand, with learning of the new environment, the neural activity undergoes changes in the primary motor cortex [54,55].

Two previous observations are specifically applicable to our results. First, it has been shown that the activity of neurons in motor areas including M1, PMd, and PMv correlates

with kinematics and dynamics of movement and there are a subset of neurons that maintain their tuning even after the force-field environment is removed, thus serve as memory cells [55–57]. Given the evidence for motion-dependency, the activity of these memory cells should correlate with kinematics of the movement. Moreover, our observation about the specificity of unlearning to the force-field structure suggests that the activity of memory cells should be tuned to motion kinematics variables that are appropriate for force-field compensation. Second, the tuning of neurons in motor cortex seems to be more sensitive to the velocity of movement compared to position, which can explain our observation of bias toward velocity during adaptation and unlearning of the combination force-fields [58].

Studies of visuomotor adaptation have shown that the M1 is engaged in late stages of learning in contrast to cerebellum which is involved in earlier stages [59]. M1 is thus hypothesized to have a role in stabilizing the memory of adaptation. In Force-field adaptation paradigms, however, results have been inconsistent. Disruption of activity in M1 via TMS seems to have no effect on the rate of adaptation and the subsequent unlearning [60]. In any case, the fact that the bias in unlearning trajectory was always toward the velocity of the movement might suggest that subpopulation of stable memory cell with better tuning to velocity of movement contribute to the temporal pattern of unlearning that we observed here.

Our current observation is consistent with previous studies [5] and suggests that the motor memory of in late stages of adaptation is more specific to the task goal compared to initial stages and this specificity remains throughout the unlearning of the adaptation memory. Previous studies have shown that the passive unlearning with time and retention of motor memory both engaged the slow process of adaptation [4, 32], specifically the amount of retention after a 24 hours period scaled with the slow component of adaptation. On the other hand, computational models of adaption have suggested that the fast state of learning contributes to early unlearning whereas slow state dominates the late unlearning [3]. We thus suspect that slow state is more specific to the goal of adaptation, thus if the same force-field is experienced on a second day without any unlearning on the first day, the

following adaptation would be more specific to the task and its corresponding gain-space trajectory would lie between the gain-space trajectories of adaptation and unlearning on the first day. We will investigate this idea in the future chapters.



## Chapter 3:

### 3.1 Introduction

In the previous chapter we showed that motor adaptation in the force-field environments was consisted of two interactive force-states that were dependent on individual movement kinematics. The contribution of these force-states to final motor output changed as subjects experienced the environment. Moreover, there was an intrinsic bias toward velocity-dependent force-state which systematically changed when the motion-dependency in the force-field changed.

A number of previous studies have suggested the role of motion-dependent force states in adaptation to force-fields [5, 36, 37]. Sing et al. [5] showed that adaptation forces can be characterized by the motion-dependent states, and the transition between different force-field environments is bounded by the interplay between the force-states. Similarly Yousif and Diedrichsen [36] demonstrated that prior exposure to a specific force-field can structurally bias the adaptation of the force-states to future force-field environments. Only Sing et al. [5] constructed a model that could capture the adaptation behavior of the individual force-states during exposure to the force-field, however, the unlearning behavior and biases in the adaptation were not captured by their model.

Here we build a computational model of motor adaptation that utilizes motion-dependent primitives as learning elements. This model combines the features from both multi-rate and viscoelastic primitive models for motor adaptation in order to capture the range of motor behaviors we observed in previous chapter. We first introduced both multi-rate and viscoelastic model and demonstrate their lack of power in predicting the aspects of unlearning and the respective biases. We next proposed a multi-rate state-dependent primitive model that was consisted of two overlapping populations of primitives with differential learning

and retention gains.

### 3.2 Multi-rate Model of Motor Adaptation

Motor adaptation to the force-field has an exponential progression. Initial exposure to the force field results in a rapid change in the motor output, which then is followed by a decrease in the rate of change. Toward the end of exposure the adaptation reaches asymptotic level. Smith et al. [3] was the first to model the motor adaptation using a state-space model with 2 states, each with different learning and retention rates. Consider adaptation to a force-field that is dependent on the velocity of the movement. The motor output on each trial can be quantified as a scalar  $y(n)$  showing the proportion of the force that is learned. The motor output on trial  $n$  can be defined combination of two states (Eq. 3.1).

$$y(n) = x_f(n) + x_s(n) \quad (3.1)$$

$$e(n) = f(n) - y(n) \quad (3.2)$$

$$\begin{cases} x_f(n+1) = A_f \times x_f(n) + B_f \times e(n) \\ x_s(n+1) = A_s \times x_s(n) + B_s \times e(n) \end{cases} \quad (3.3)$$

On trial  $n$ ,  $e(n)$  is the error between desired motor output,  $f(n)$  and current output  $y(n)$  (Eq. 3.2). The motor output is generated by combining two hidden state, fast and slow states, which are represented as  $x_f(n)$  and  $x_s(n)$  respectively (Eq. 3.3). For each state, a coefficient defines the rate of learning from the error and a second coefficient defines the proportion of state retained from previous trial. The fast state learns from the error efficiently but poorly retains the previous state. On the other hand, the slow state is sluggish in learning from the error, but is able to retain the previous state. The difference between these two states can be formulated by the relationship between the pairs  $(A_s, A_f)$  as well as  $(B_f, B_s)$  (Eq. 3.4 and 3.5).

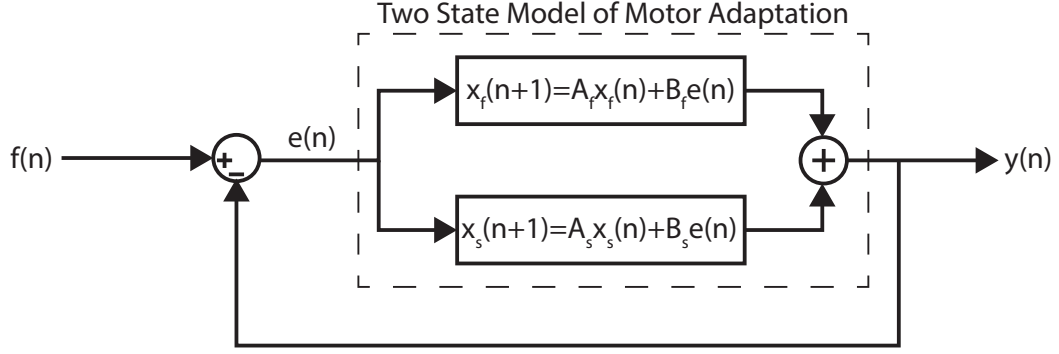


Figure 3.1: The input to the system is the adaptation goal of the environment. For the baseline period the input is zero, but is non-zero in force-field period. The learning in the system is mediated by the error between adaptation goal and current motor output on each trial. Two hidden state  $x_f$  and  $x_s$  learn from the error separately and their combined outputs creates the next trial motor output. The unlearning period is triggered in the system by forcing the error  $e(n)$  to zero.

$$\text{retention factor} : 1 > A_s > A_f \quad (3.4)$$

$$\text{learning rate} : 1 > B_f > B_s \quad (3.5)$$

We can demonstrate the multi-rate model of motor adaptation as two parallel processes that learn from the error in a feedback setting. Fig. 3.1 shows this parallel realization.

### 3.2.1 Response Characteristics of Multi-rate Model of Motor Adaptation to Force-fields

Here we simulated the multi-rate model in a force-field paradigm similar to chapter 2. The force-field environment was modeled as a step input  $f(n) = u(n - 15)$  to the system shown in Fig. 3.1. Importantly we modeled the unlearning after adaptation period by forcing the error signal  $e(n)$  to 0. This resulted in a decay of output  $y(n)$  which was the result of the retention coefficients  $A_s$  and  $A_f$ .

In order to explore the interaction between states of the multi-rate model, we looked the evolution of fast and slow states during adaptation and unlearning periods (Fig. 3.3).

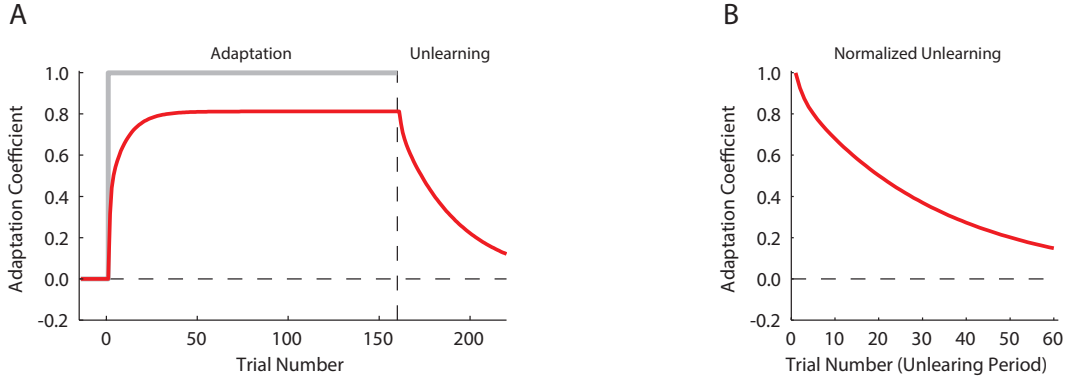


Figure 3.2: (A) The force-field is applied at trial 1 and remains for 165 trials, shown by the gray solid line. During the baseline period (negative trial numbers) the motor adaptation level is at zero. However when the force-field is applied, motor output reaches a new asymptotic level. Initial the change in the motor adaptation is fast (trials 1 to 50). This change becomes smaller as adaptation reaches to late phases (trials 100 to 165). With the start of unlearning period, the adaptation coefficient gradually reverts back to the baseline level. The start of unlearning period is shown as a vertical dashed-line.(B) Normalized unlearning of adaptation to the force-field. The normalized unlearning was calculated by scaling adaptation coefficient with respect to the first point in the period. Thus the first point is rescaled to 1.

The fast state contributed to the majority of the output in early adaptation, given that the error between the motor output and force-field was the largest. However, as adaptation progressed, the amplitude of the motor error decreased, and as a result the contribution of fast state declined while the contribution of slow state continually increased. This can be observed in Fig. 3.3A, where the initial peak in the output of fast state was followed by a gradual decline. When the unlearning period started, the input to the multi-rate model was clamped at 0, and the poor retention factor  $A_f$  caused a rapid decline in the output of the fast state towards the baseline (Fig. 3.3E and F).

The slow state exhibited a different behavior compared to the fast state (Fig. 3.3C and D). First, the exposure to force-field resulted in a gradual growth towards the new adaptation goal. Unlike the fast state, the slow state contributed minimally in early adaptation, due to poor learning rate. By the end of adaptation, the slow state contributed to the majority of the motor output instead. Having a good memory of its previous state, this

state consistently approached the adaptation goal. Second, the unlearning period resulted in the decay of adaptation in slow state, however, the decay was much slower, and by the end of unlearning period most of the motor output was consisted of the slow state output.

Although the multi-rate model was successful in capturing the overall adaptation behavior, it ignores the dependency of the motor output to different motion kinematics. In chapter 2 we have shown that the motor output can be reconstructed from force-states that are dependent on position and velocity of movement on individual trials. The multi-rate model as, a one-dimensional model, cannot capture the differences in the evolution of these force-states during adaptation and unlearning of the force-fields. Therefore we next explored viscoelastic primitive model for motor adaptation that takes into account different movement kinematics in final output [5].

### 3.3 Viscoelastic Primitive Model for Motor Adaptation

The motivation for the viscoelastic primitive model came from the observation that during adaptation to the motion-dependent force-fields, subject's compensatory force contained components from individual kinematic parameters. In contrast to the multi-rate model, this model can capture multiple dimensions of the motor output. Here, we first introduce the viscoelastic primitive model first proposed by [5], and then analyze its power in capturing the features of adaptation and the unlearning previously shown in chapter 2.

The viscoelastic primitive model is consisted of a set of motor primitives that are uniquely tuned to movement kinematics variables, such as position and velocity. Consider a set of  $n$  distinct primitives, which receive the temporal profile of movement kinematics (Fig. 3.4). Moreover, consider that the motor output on current trial is a weighted sum of the individual primitive force outputs.

We can assume that each primitive is linearly dependent on position and velocity of the movement. This dependency can be represented as a point in a 2 dimensional space where each axis represents a individual movement kinematic variable. Thus, we can identify primitive  $S_i$  with  $[K_i, B_i]$  where  $K_i$  is the gain for the position, and  $B_i$  is the gain for the

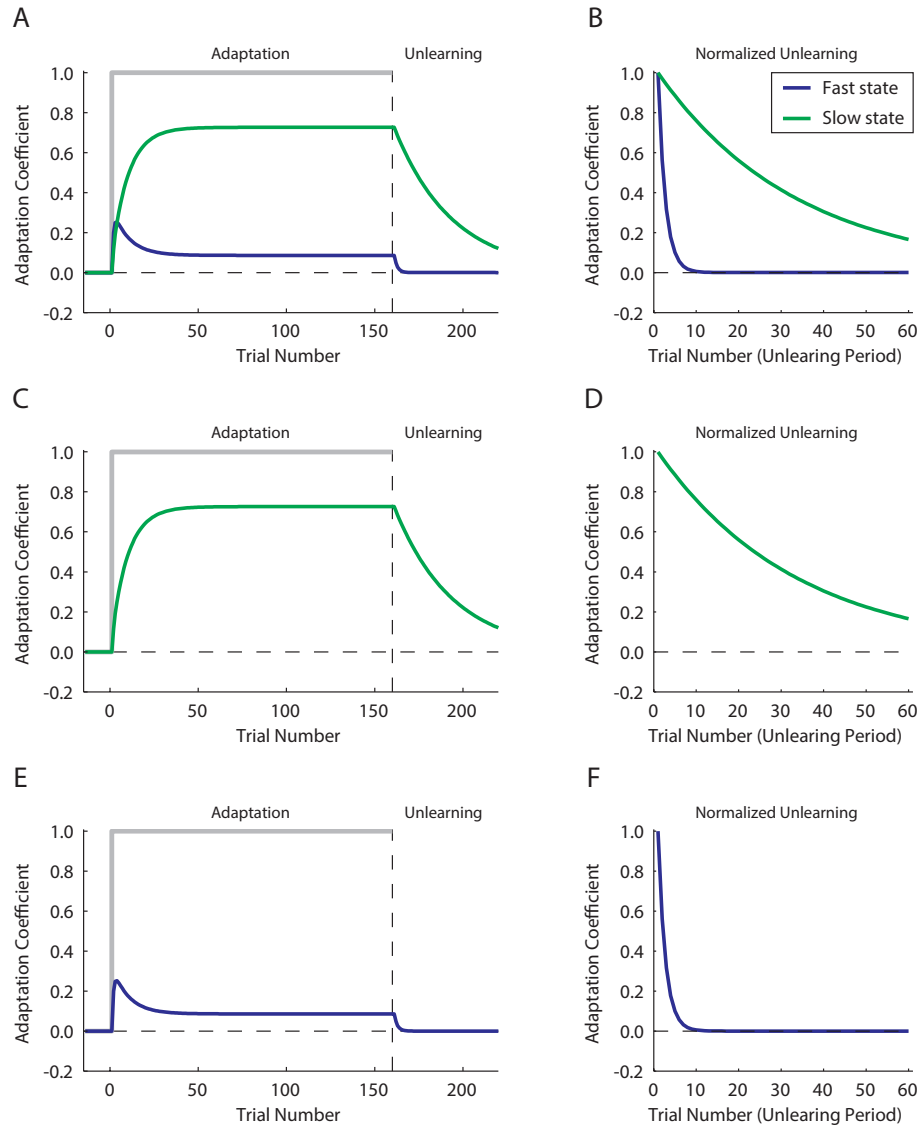


Figure 3.3: (A,C,E) The force-field is applied at trial 1 and remains for 165 trials, shown by the gray solid line. (A) Comparison between the evolution of the fast and slow states during adaptation to the force-field. The fast state is more active during early phase of adaptation (blue solid line), however slow state takes over in late phases (green solid line). During the unlearning period both states gradually revert back towards baseline level, however the decay of the fast state is more rapid when compared to the slow state. The start of unlearning period is shown as a vertical dashed-line. (B) Normalized unlearning for adaptation for both fast and slow states. The normalized unlearning was calculated by scaling adaptation coefficient of each state with respect to the first coefficient in the period. Thus the first point is rescaled to 1. The decay of the fast state is faster compared to slow state when both states start from the same point. (C and D) Adaptation and unlearning behavior of the slow state.(E and F) Adaptation and unlearning behavior of fast state.

velocity of the movement, respectively. Fig. 3.5 shows the input/output relationship for an example primitive in this space.

The learning in the viscoelastic primitive model is mediated by the difference between the goal motor output vector and the current motor output vector. Consider the goal motor output  $y^*$  and current motor output  $y$  that are defined in  $R^{2 \times 1}$ . As an example, the position-dependent force-field goal is  $[1, 0]^T$  and the velocity-dependent force-field goal is  $[0, 1]^T$ . On each trial, the motor output is defined as Eq. 3.6.

$$y = \sum_{i=1}^N W_i \times \begin{bmatrix} K_i \times P \\ B_i \times V \end{bmatrix} \quad (3.6)$$

Given that the position and velocity of movement are applied to all primitives in a same manner, they can be omitted from the Eq. 3.6 and the motor output can be simplified (Eq. 3.7 and 3.8).

$$y = \sum_{i=1}^N W_i \times \begin{bmatrix} K_i \\ B_i \end{bmatrix} \quad (3.7)$$

$$y = \sum_{i=1}^N W_i \times S_i \quad (3.8)$$

In Eq. 3.8 the output  $y$  can be altered by changing the gains  $W_i$ . A first order gradient decent rule can be used to update the weights for the primitives in order to reduce the error between the motor output and the goal of adaptation (Eq.3.9).

$$\Delta W_i = \eta (y^* - y)^T S_i \quad (3.9)$$

In this equation  $\eta$  is the constant for learning. The amount of change in the weight depends on the angle between the primitive  $S_i$  and the error  $y^* - y$ . If the angle is close

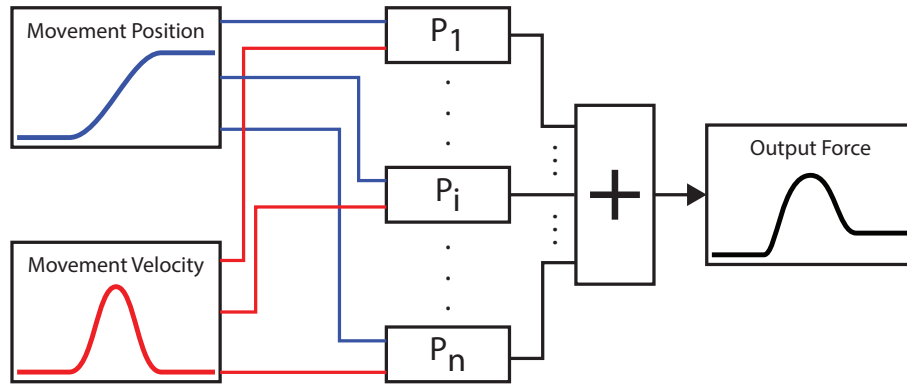


Figure 3.4: A population of  $n$  primitives receive kinematics information regarding both the position and velocity of the movement which are shown blue and red respectively. The output of these primitives are combined to create the force output, shown in black trace.

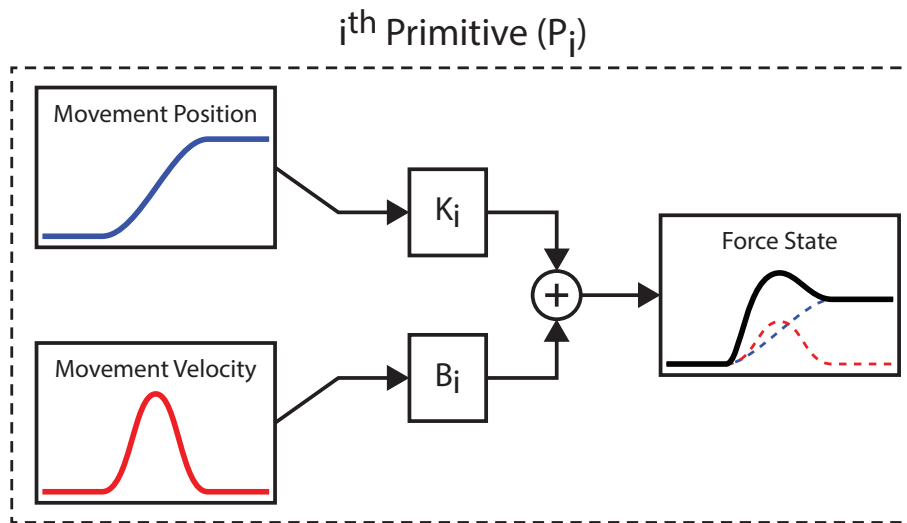


Figure 3.5: The position variable of the movement is weighted with the gain  $K_i$ , whereas the velocity of the movement is weighted with the gain  $B_i$ . The weighted position and velocity variables are then combined to create the force-state output of the primitive.



to  $90^\circ$ , the change in the weight is minimal, and if the angle is close to  $0^\circ$  the change is maximal. As a result, the learning for each primitive is dependent on its location in the gain-space, the adaptation goal, and the current state of motor adaptation. Thus, for a fix adaptation goal and an initial state, the evolution of motor output depends on the distribution of the primitive in the space.

### 3.3.1 Simulation of Viscoelastic Model in Force-field Adaptation and Un-learning

Sing et al.[5] previously have shown that viscoelastic model can capture the subjects' behavior during adaptation to different motion-dependent force-fields, however the unlearning behavior has not been explored yet. We extended Eq. 3.9 and included a term to account for the inter-trial stability in the memory of the weights. The weights on trial  $n + 1$  can relate to trial  $n$  in the following way (Eq. 3.10).

$$W_i^{(n+1)} = (1 - \alpha) W_i^{(n)} + \Delta W_i^{(n)} \quad (3.10)$$

In this equation, the term  $\alpha$  represents the proportion of memory that is forgotten in transition from trial  $n$  to  $n + 1$ . For example, when  $\alpha = 0$  the motor system has a perfect memory of weights. However previous observation showed that the adaptation memory gradually decays over time or trial and in reality  $\alpha > 0$ . We thus simulate the viscoelastic primitive model with an  $\alpha > 0$ .

We define a viscoelastic model with population of 5000 primitives. The primitives we drawn from a jointly normal distributions equal variances along position-dependent and velocity-dependent gains with correlation of 0.8 between them (Eq.3.11 and 3.12) [5].

$$\begin{bmatrix} K_i \\ B_i \end{bmatrix} \sim \mathcal{N}(\mu, \Sigma) \quad \mu = [0, 0] \quad (3.11)$$

$$\Sigma = \begin{bmatrix} \sigma_p^2 & \rho \cdot \sigma_p \cdot \sigma_v \\ \rho \cdot \sigma_p \cdot \sigma_v & \sigma_v^2 \end{bmatrix} \quad \sigma_p = \sigma_v, \quad \rho = 0.8 \quad (3.12)$$

First we demonstrate the adaptation and unlearning behavior of viscoelastic model for position-FF and velocity-FF (Fig. 3.6). The model makes two critical predictions about the motor adaptation pattern. First, the adaptation trajectories for position-dependent and velocity dependent force-force fields have similar shapes. Second, the unlearning trajectories are straight lines towards the origin. However, as shown in chapter 2, adaptation trajectory for velocity force field is closer to velocity axis, thus more aligned to goal compared to position-dependent force-field adaptation. In addition, the unlearning trajectories were not simple lines towards the origin. The curvature in the unlearning trajectories suggests that the memory of velocity-aligned and position-aligned components decay at different rates depending on the force-field environment.

To further illustrate the behavior in one-state viscoelastic primitive model, we simulate two now combination force-field environments similar to the experiments in chapter 2. Figures (3.7) and (3.8) show the adaptation and unlearning prediction for the combination-FF and a position-biased-FF, respectively.

The difference between model predictions and experimental results for unlearning trajectories is more evident in this case. The model fails to show the emergence of a bias toward velocity-dependent force-state. Even though the one-state viscoelastic model mimics the shape of adaptation trajectory for pure position and velocity dependent force-fields, it is not capable of capturing the aspects of their unlearning trajectories. Moreover, the behavior of motor system during adaptation and unlearning of combination force-field is not predicted by viscoelastic model.

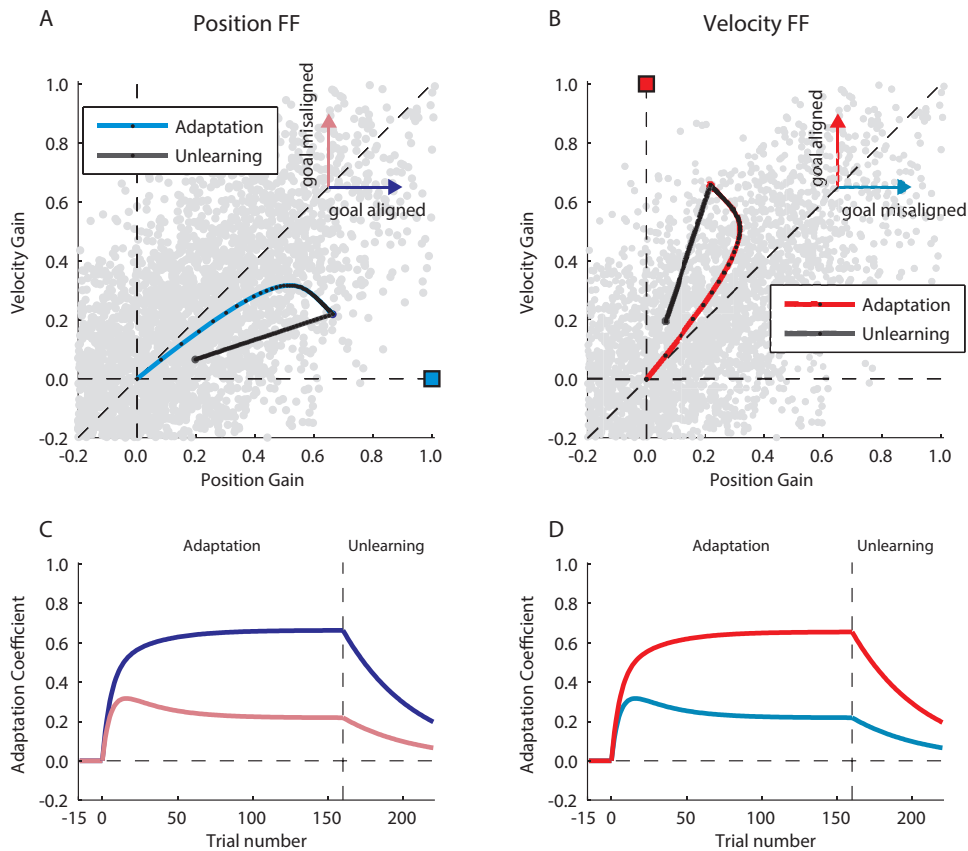


Figure 3.6: (A) Evolution of position and velocity gains during adaptation and unlearning of Position-FF, gain trajectories during adaptation and unlearning periods are shown in blue and gray, respectively. The adaptation goal is shown as a blue filled rectangle. Each gain can be broken down to goal-aligned and goal misaligned components, as shown by two vectors. (B) Evolution of position and velocity gains during adaptation and unlearning of a velocity-FF. Adaptation gains are shown in red, and unlearning gains in gray. Goal of adaptation is represented as a red square. Here direction of the goal aligned and goal misaligned components of each gain are shown as a red and cyan arrow, respectively. (C,D) the temporal changes for goal-aligned and goal-misaligned components are shown for each force field environment in A and B.

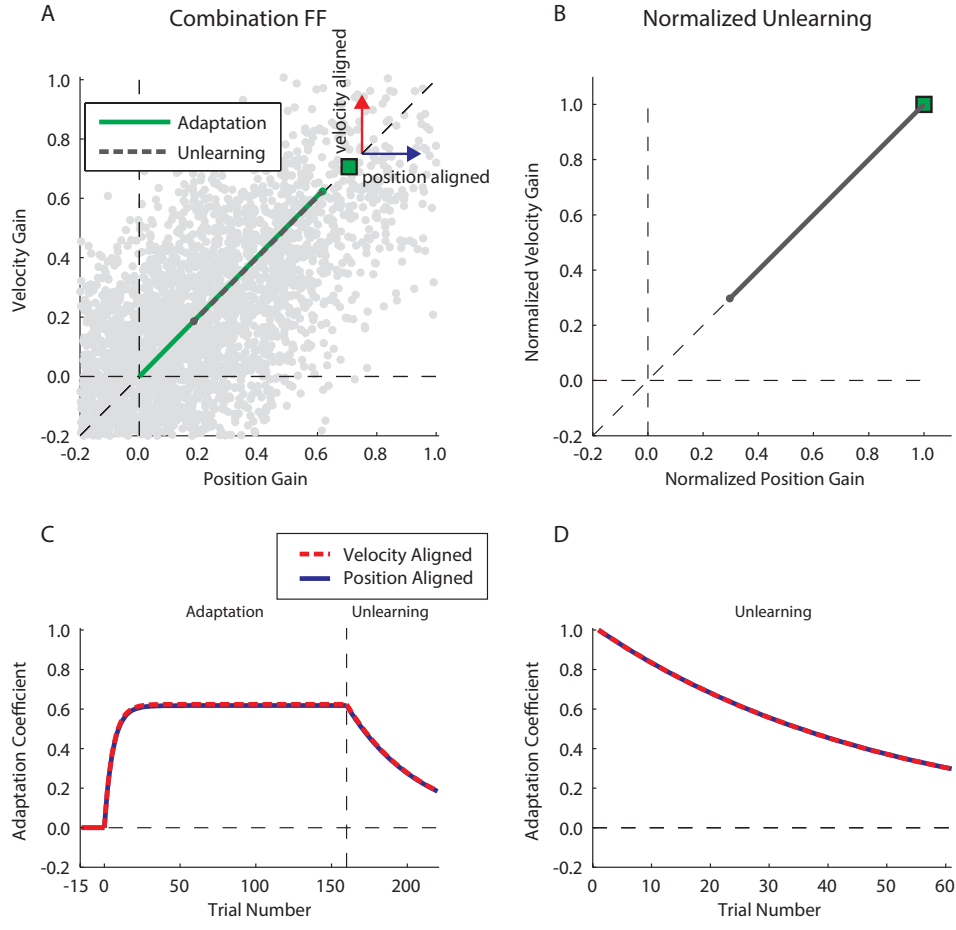


Figure 3.7: (A). adaptation gains are shown with green solid line, whereas unlearning gains are shown by gray dashed line. Here the goal of adaptation is shown by a green square and located at  $x=y$  line. The directions of position-aligned and velocity-aligned components are shown by blue and red arrow respectively.(B). The normalized unlearning gains were computed by rescaling the gains during unlearning by their respective starting points, thus the first point is rescaled to  $[1,1]$  in gain space. The gray line represents the normalized unlearning. (C). Temporal changes in position-aligned and velocity-aligned gains during adaptation and unlearning of the combination force-field. Position aligned gains are shown in blue and velocity-aligned gains are shown in dashed red line (D). Normalized unlearning of position and velocity aligned gains.

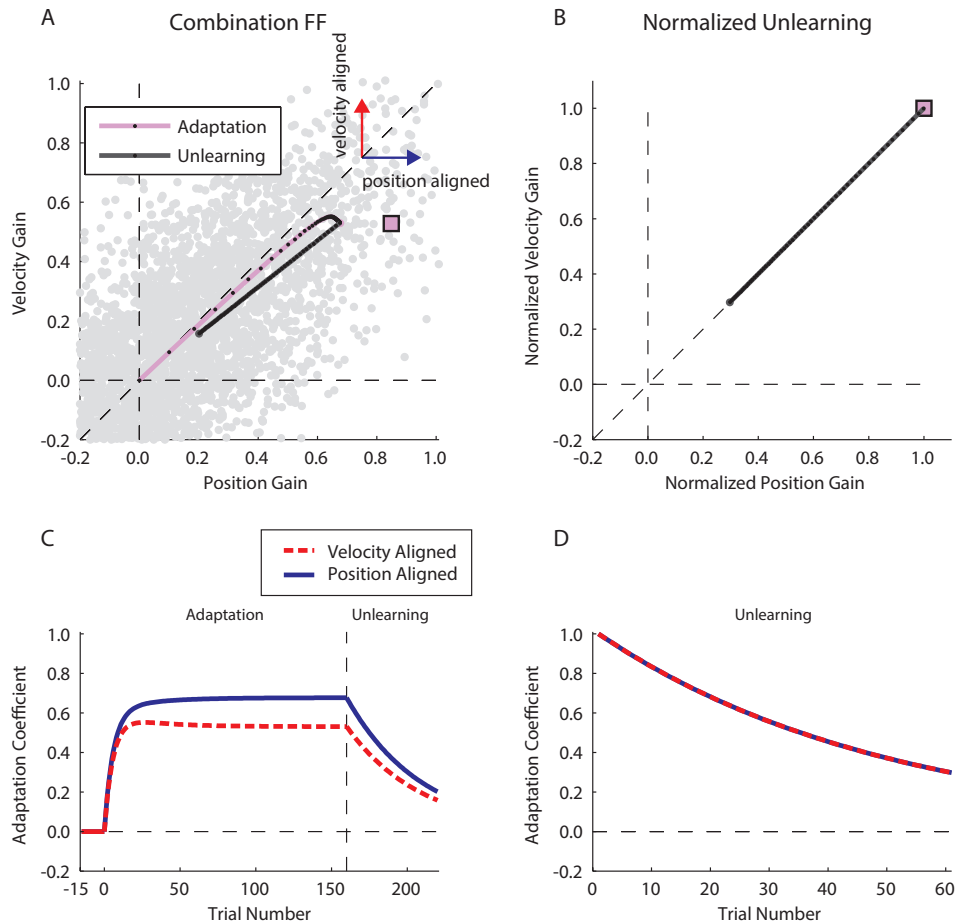


Figure 3.8: (A). adaptation gains are shown with purple solid line, whereas unlearning gains are shown in gray dashed line. Here the goal of adaptation is shown by a filled purple square and located at in a region of gain space with larger position gain than velocity. For each gain the direction of position aligned and velocity aligned component are shown by blue and red arrow respectively. (B). the normalized unlearning gains were computed by rescaling the gains by their respective start points value, the unlearning starts from point [1,1] in gain space. The gray line represents the normalized unlearning of gains (C). temporal changes in position-aligned and velocity-aligned gains during adaptation and unlearning of the position-biased force-field. Position aligned gains are shown in blue and velocity-aligned gains are shown in red. The bar graph shows the comparison between position-aligned and velocity-aligned gains at the points selected in left panel, (D). Normalized unlearning of position and velocity aligned gains.

### 3.4 Multi-rate State-dependent Primitive Model for Motor Adaptation

In previous sections we showed that both viscoelastic primitive and multi-rate models had limited power in explaining the motor behavior. We wondered whether these two models were elements of a more general model that could explain the behavior of motor system during both force-field adaptation and unlearning in a unified scheme.

We hypothesized that the motor system output was the result interaction between two primitive spaces with distinct learning and retention rates. Consider two primitive spaces  $S_{slow}$  and  $S_{fast}$ . Each primitive  $i$  in space  $S_{slow}$  is tuned to position and velocity of movement with the a unique gain vector  $[K_{slow}^i, B_{slow}^i]$ . Similarly, a primitive  $i$  in  $S_{fast}$  is tuned to movement kinematic with  $[K_{fast}^i, B_{fast}^i]$ . The force-state from each space can be described as follows (Eq. 3.13 and 3.14).

$$x_{slow}^n = \sum_{i=1}^n [W_{slow}^i]^n \times \begin{bmatrix} K_{slow}^i \times P \\ B_{slow}^i \times V \end{bmatrix} \quad (3.13)$$

$$x_{fast}^n = \sum_{i=1}^n [W_{fast}^i]^n \times \begin{bmatrix} K_{fast}^i \times P \\ B_{fast}^i \times V \end{bmatrix} \quad (3.14)$$

$$y^n = x_{slow}^n + x_{fast}^n \quad (3.15)$$

In the force-field environment,  $y^*$  can represent the goal of adaptation and similar to previous case and the error between the goal and current motor output can be defined as  $e = y^* - y^n$ . The learning can be defined in terms of updating of the weights for both primitive spaces (Eq. 3.16 and 3.17).

$$[\Delta W_{slow}^i]^n = \eta(y^* - y)^T S_{slow}^i \quad (3.16)$$

$$[\Delta W_{fast}^i]^n = \eta(y^* - y)^T S_{fast}^i \quad (3.17)$$

Finally, assuming that the weight change in response to error and subsequent decay rates are distinct for each primitive space, the new set of weights for each primitive space can be calculated (Eq. 3.18 and 3.19).

$$[W_{slow}^i]^{(n+1)} = (1 - \alpha_{slow}) \times [W_{slow}^i]^{(n)} + \beta_{slow} \times [\Delta W_{slow}^i]^n \quad (3.18)$$

$$[W_{fast}^i]^{(n+1)} = (1 - \alpha_{fast}) \times [W_{fast}^i]^{(n)} + \beta_{fast} \times [\Delta W_{fast}^i]^n \quad (3.19)$$

The interaction between the learning and retention rates in this model determines how fast the model adapts to the perturbation and how stable the memory of this adaptation will be. In addition, the shape of each primitive space delineates a specific adaptation trajectory that is in the direction maximum error reduction. In the next two sections we explored the behavior of this model under different force-field conditions when the primitive spaces have similar or distinct distributions in the motion-dependent gain space.

### 3.4.1 Multi-rate State-dependent Primitive Model with Same Distribution

First we assumed that the distributions for slow and fast primitive spaces were similar (Eq. 3.20).

$$S_{fast}^i = S_{slow}^i = \begin{cases} K_{fast}^i = K_{slow}^i \\ B_{fast}^i = K_{slow}^i \end{cases} \quad (3.20)$$

Similar to viscoelastic primitive model, we built two primitive spaces with population of 2500 each, from one joint normal distributions (Eq. 3.21 and 3.22).

$$\mathcal{N}_{fast}(\mu_{fast}, \Sigma_{fast}) = \mathcal{N}_{slow}(\mu_{slow}, \Sigma_{slow}) = \mathcal{N}(\mu, \Sigma) \quad \mu = [0, 0] \quad (3.21)$$

$$\Sigma = \begin{bmatrix} \sigma_p^2 & \rho \cdot \sigma_p \cdot \sigma_v \\ \rho \cdot \sigma_p \cdot \sigma_v & \sigma_v^2 \end{bmatrix} \quad \sigma_p = \sigma_v, \quad \rho = 0.8 \quad (3.22)$$

Given the similarity between the gain distributions in viscoelastic model and current implementation of multi-rate state-dependent model, any change in adaptation trajectories should be caused by the difference in learning and retention rates between the two populations. First we simulated the model under pure position or velocity dependent force-fields.

As shown in Fig. 3.9, the asymmetries in the adaptation trajectories could not be reproduced only by implementation of distinct learning and retention rates. In chapter 2 we observed that biases were more evident under combination force-field environments. So we also simulate the model under both the combination-FF and the position-biased-FF.

Fig. 3.11 and 3.12 clearly demonstrated that the multi-rate state-dependent primitive mode with similar distributions was not capable of exhibiting the biases in the trajectories, particularly during unlearning of the combination force-fields.

We wondered whether the distribution of primitive spaces could mediate any asymmetric association between motion dependent force-field and motor adaptation. The experimental result showed that the gain trajectories for combination force-field were biased toward the velocity gain. Moreover, a closer look at the gain-trajectories for these two force-fields reveals that the degree of asymmetry was dependent on the trial number in both adaptation and unlearning periods. In both early adaptation and unlearning, the trajectories favored symmetric distribution, however towards the end of each period the asymmetry behavior dominated the trajectories. this could be linked to the prediction of the two-rate model that early phases of learning and unlearning is affected by both fast and slow states, whereas late phases were mostly influenced by the behavior of slow state.

Combining these two observations, we made two critical assumptions about the multi-rate state-dependent primitive model. First, the distributions of fast and slow primitives



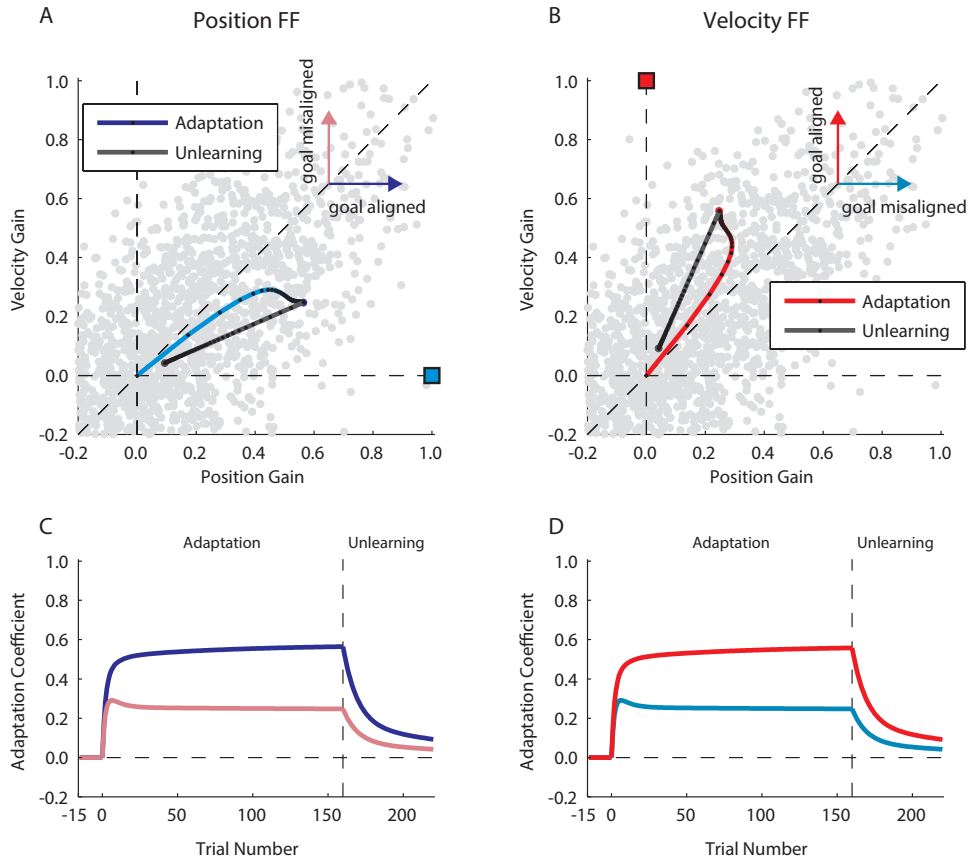


Figure 3.9: (A) Evolution of position and velocity gains during adaptation and unlearning of Position-FF, gain trajectories during adaptation and unlearning periods are shown in blue and gray, respectively. The adaptation goal is shown as a blue filled square. Each gain can be broken down into goal-aligned and goal misaligned components, as shown by the two vectors. (B) Evolution of position and velocity gains during adaptation and unlearning of a velocity-FF. Adaptation gains are shown in red, and unlearning gains in gray. Goal of adaptation is represented as a red square. Here direction of the goal aligned and goal misaligned components of each gain are shown by red and cyan arrows, respectively. (C,D) The temporal changes for goal-aligned and goal-misaligned components are shown for each force field environment in A and B.

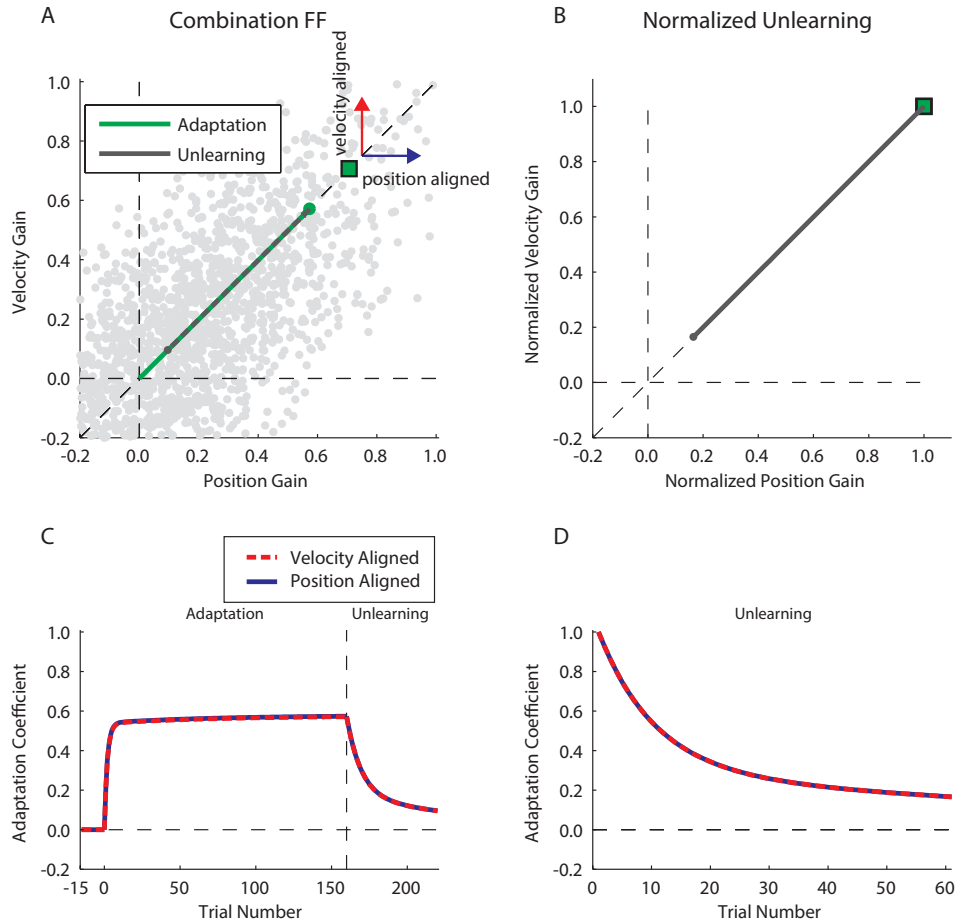


Figure 3.10: (A) Adaptation gains are shown with green solid line, whereas unlearning gains are shown by gray dashed line. Here the goal of adaptation is shown by a green square and located at  $x=y$  line. The directions of position-aligned and velocity-aligned components are shown by blue and red arrows respectively. (B) The normalized unlearning gains were computed by rescaling the gains during unlearning by their respective starting points, thus the first point is rescaled to  $[1,1]$  in gain space. The gray line represents the normalized unlearning. (C) Temporal changes in position-aligned and velocity-aligned gains during adaptation and unlearning of the combination force-field. Position aligned gains are shown in blue and velocity-aligned gains are shown in dashed red line. (D) Normalized unlearning of position and velocity aligned gains.

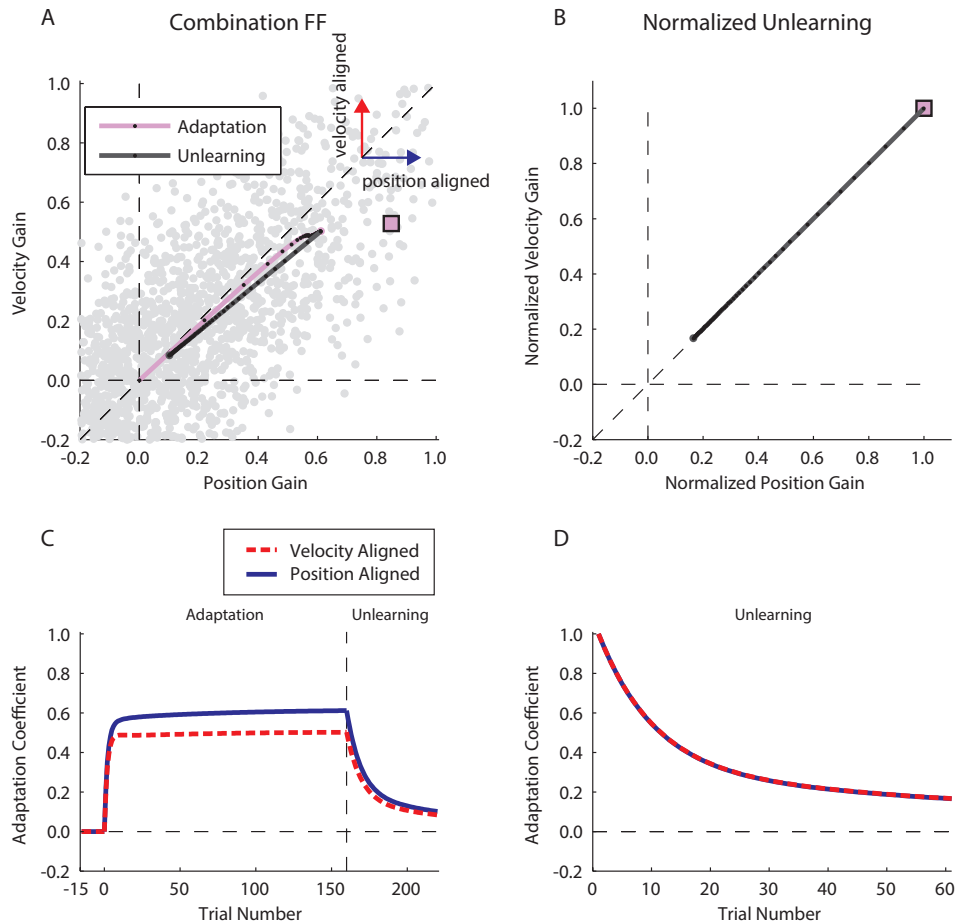


Figure 3.11: (A) Adaptation gains are shown with purple solid line, whereas unlearning gains are shown in gray solid line. Here the goal of adaptation is shown by a filled purple square and located at in a region of gain space with larger position gain than velocity. For each gain the direction of position aligned and velocity aligned component are shown by blue and red arrows, respectively. (B) The normalized unlearning gains were computed by rescaling the gains by their respective start points value, the unlearning starts from point [1,1] in gain space. The gray line represents the normalized unlearning of gains. (C) Temporal changes in position-aligned and velocity-aligned gains during adaptation and unlearning of the position-biased force-field. Position aligned gains are shown in blue and velocity-aligned gains are shown in red. The bar graph shows the comparison between position-aligned and velocity-aligned gains at the points selected in left panel. (D) Normalized unlearning of position and velocity aligned gains.

were not essentially similar. Second, the asymmetries in the trajectories should be modulated by the distribution of slow primitives.

### 3.4.2 Multi-rate state-dependent primitive model with distinct distributions

Here we altered the primitive distributions for multi-rate state-dependent primitive model in order to test whether the biases in the experimental findings could be reproduced. First, we assumed that the fast state distribution was aligned to the mid-line of the primitive space, similar to previous case. More importantly, we assumed that the slow state distribution was mostly aligned with velocity axis of the space. This required that the variance along  $B_{slow}$  ( $\sigma_v$ ) to be larger than  $K_{slow}$  ( $\sigma_p$ ), and the correlation between the two variances be small enough. We first modified the distribution for fast primitives (Eq. 3.23 and 3.24).

$$\begin{bmatrix} K_{fast}^i \\ B_{fast}^i \end{bmatrix} \sim \mathcal{N}_{fast}(\mu_{fast}, \Sigma_{fast}) \quad \mu_{fast} = [0, 0] \quad (3.23)$$

$$\Sigma_{fast} = \begin{bmatrix} \sigma_p^2 & \rho \cdot \sigma_p \cdot \sigma_v \\ \rho \cdot \sigma_p \cdot \sigma_v & \sigma_v^2 \end{bmatrix} \quad \sigma_p = \sigma_v = 0.547 \quad , \quad \rho = 0.257 \quad (3.24)$$

Unlike fast primitive, we changed the distribution for slow primitive and biased the variability towards the velocity axis in the gain space (Eq.3.25 and 3.26).

$$\begin{bmatrix} K_{slow}^i \\ B_{slow}^i \end{bmatrix} \sim \mathcal{N}_{slow}(\mu_{slow}, \Sigma_{slow}) \quad \mu_{slow} = [0, 0] \quad (3.25)$$

$$\Sigma_{\text{slow}} = \begin{bmatrix} \sigma_p^2 & \rho \cdot \sigma_p \cdot \sigma_v \\ \rho \cdot \sigma_p \cdot \sigma_v & \sigma_v^2 \end{bmatrix} \quad \sigma_p = 0.2812 \quad \sigma_v = 0.567 \quad , \quad \rho = 0.008 \quad (3.26)$$

The simulation of the multi-rate state-dependent primitive model could capture the asymmetries presented in the experimental data. This is shown in Fig. 3.12.

The multi-rate state-dependent primitive model seemed to capture both the adaptation and unlearning behaviors for the position and velocity-dependent force-fields. The adaptation trajectory for velocity dependent force-field was closer to the velocity axis. In addition unlearning trajectory closely follows the axis.

We also analyzed the evolution of the gain trajectories under two combination force-field environments. Fig. 3.13 and 3.14 show the result for each force-field.

The trajectories in combination-FF and position-biased-FF clearly exhibited similar behavior to experimental finding. Adaptation and unlearning trajectories were biased toward velocity axis for the combination force-field. For combination-FF, the unlearning was appropriately biased towards the velocity axis. In addition, during the unlearning of position-biased force-field, initially the trajectory had more position-dependent contribution, but the velocity-dependent state dominated the trajectory towards the end of the period.

In order to demonstrate how each primitive contributes to the shape of the trajectory, we next looked at the progression of slow and fast primitives in gain-space of adaptation. We observed that for both combination force-fields, the learning of fast state was mainly aligned with the mid-line of the space and was in the direction of the adaptation goal. This was contrasted with the trajectory of the slow state which was shifted toward the velocity axis of space (Fig. 3.15 and 3.16).

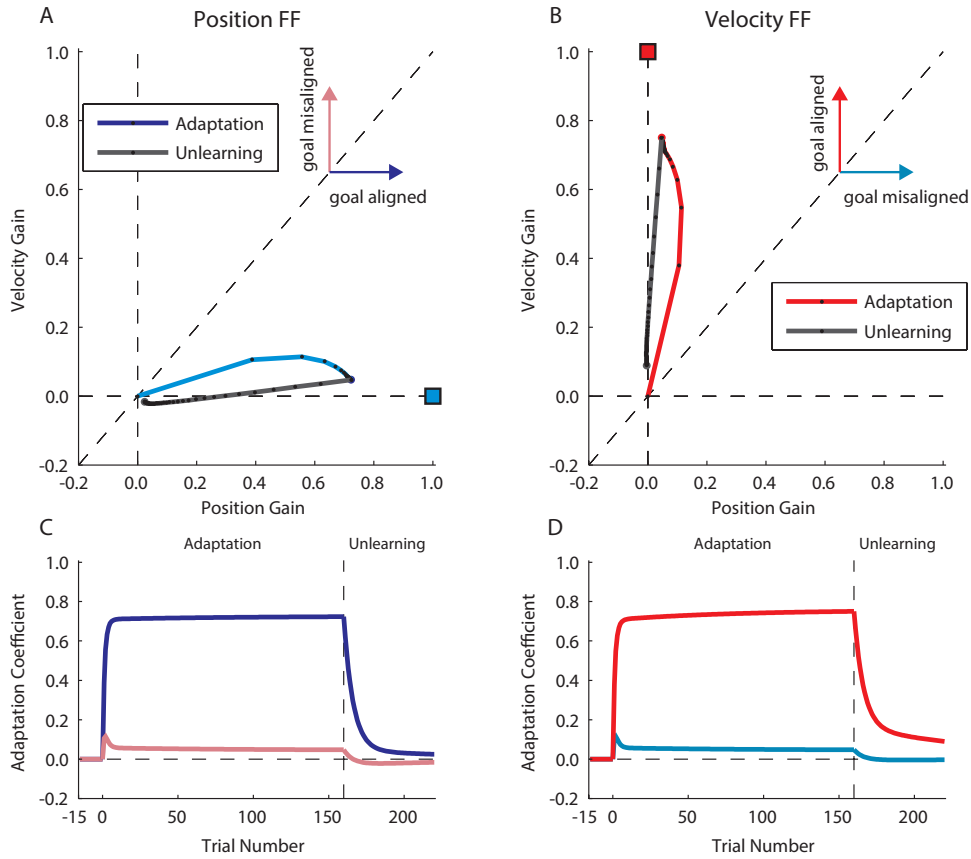


Figure 3.12: (A) Gain trajectories during adaptation and unlearning periods are shown in blue and gray, respectively. The adaptation goal is shown as a blue filled square. Each gain can be broken down to goal-aligned and goal misaligned components, as shown by two vectors. (B) Evolution of position and velocity aligned gains during adaptation and unlearning of a velocity-FF. Adaptation gains are shown in red, and unlearning gains in gray. Goal of adaptation is represented as a red square. Here direction for the goal aligned and goal misaligned components are shown as a red and cyan arrows, respectively. (C,D) the temporal changes for goal-aligned and goal-misaligned components are shown for each force field environment in A and B.

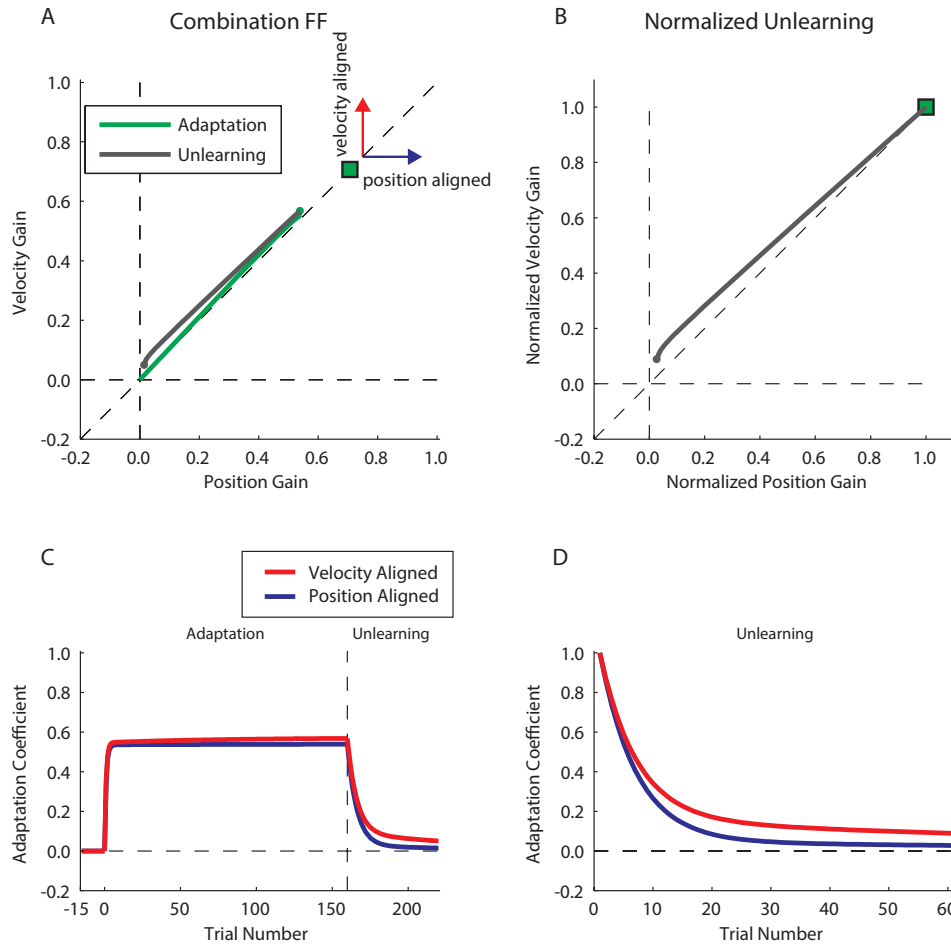


Figure 3.13: (A) Adaptation gains are shown with green solid line, whereas unlearning gains are shown by gray dashed line. Here the goal of adaptation is shown by a green square and located at  $x=y$  line. The directions of position-aligned and velocity-aligned components are shown by blue and red arrow respectively. (B) The normalized unlearning gains were computed by rescaling the gains during unlearning by their respective starting points, thus the first point is rescaled to [1,1] in the gain space. The gray line represents the normalized unlearning. (C) Temporal changes in position-aligned and velocity-aligned gains during adaptation and unlearning of the combination force-field. Position aligned gains are shown in blue and velocity-aligned gains are shown in dashed red line. (D) Normalized unlearning of position and velocity aligned gains.

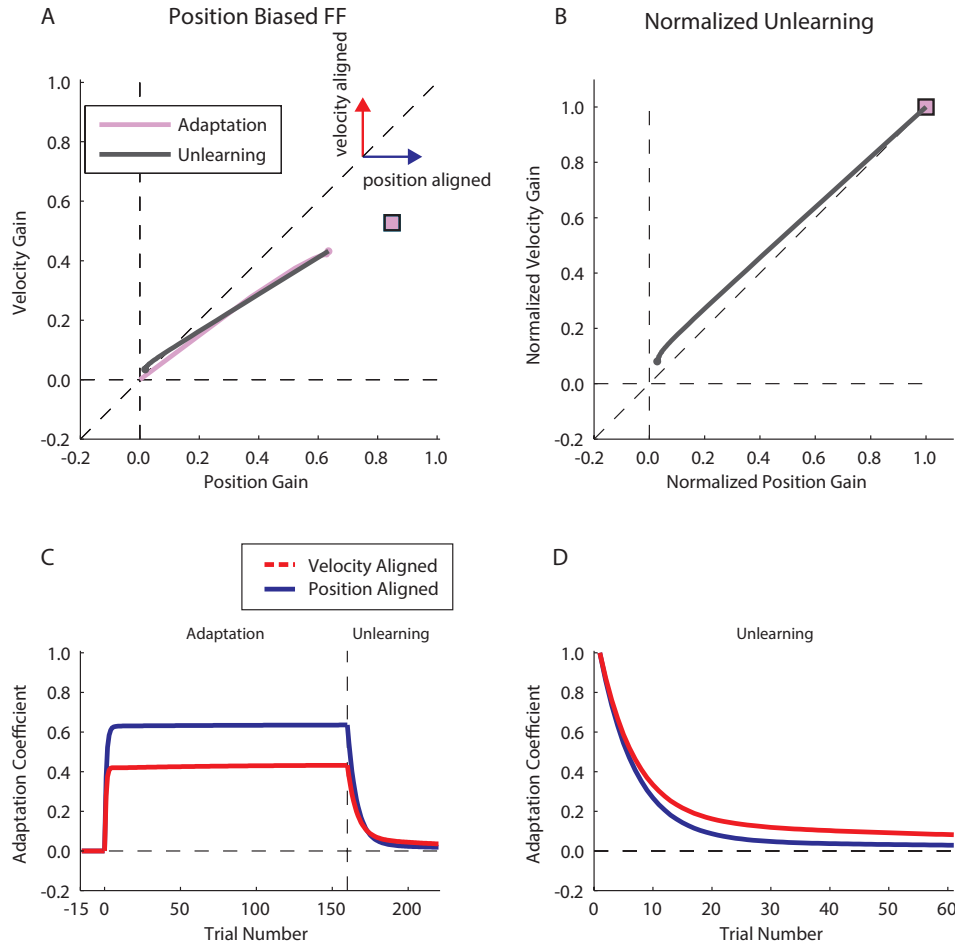


Figure 3.14: (A) Adaptation gains are shown with purple solid line, whereas unlearning gains are shown in gray dashed line. Here the goal of adaptation is shown by a filled purple square and located at in a region of gain space with larger position gain than velocity. For each gain the direction of position aligned and velocity aligned component are shown by blue and red arrow respectively. (B) The normalized unlearning gains were computed by rescaling the gains by their respective start points value, the unlearning starts from point [1,1] in gain space. The gray line represents the normalized unlearning of gains. (C) Temporal changes in position-aligned and velocity-aligned gains during adaptation and unlearning of the position-biased force-field. Position aligned gains are shown in blue and velocity-aligned gains are shown in red. (D) Normalized unlearning of position and velocity aligned gains.



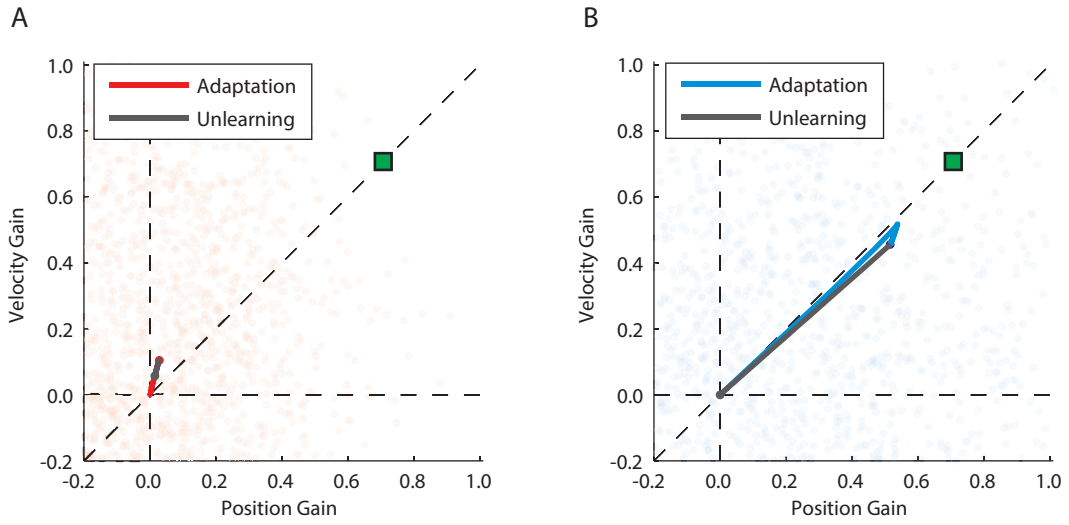


Figure 3.15: (A) Adaptation and unlearning of slow primitive in gain space. The goal of adaptation is shown by a filled green square. The distribution of primitives is shown by red circles in gain space. (B) Adaptation and unlearning of slow primitive in gain space. The goal of adaptation is shown by a filled green square. The distribution of primitives is shown by red circles in gain space.

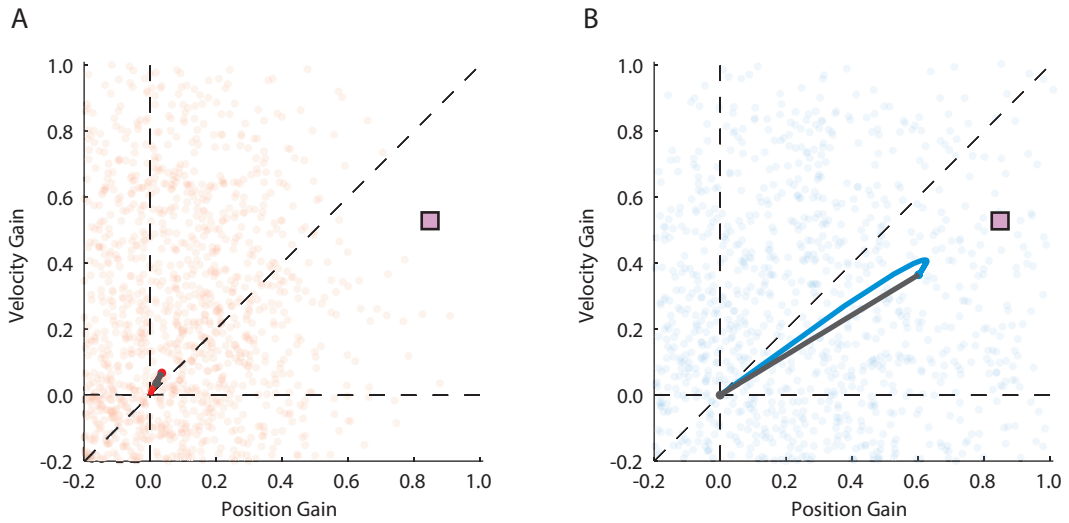


Figure 3.16: (A) Adaptation and unlearning of slow primitive in gain space. The goal of adaptation is shown by a filled purple square. The distribution of primitives is shown by red circles in gain space. (B) Adaptation and unlearning of slow primitive in gain space. The goal of adaptation is shown by a filled green square. The distribution of primitives is shown by red circles in gain space.

## 3.5 Discussion

Here we have shown that the behavior of the motor system when adapting and subsequently unlearning a force-field can be effectively explained by a multi-rate state-dependent primitive model that has two key characteristics. First, the model contained two distributions of primitives, one set of primitives was efficient in learning from the error but has poor ability in retaining the learned pattern, referred to as fast primitive, while the other set of primitives, slow primitive, had low sensitivity to the error but had good memory of the previous learned pattern. Second, the distributions for these primitive were not similar in the gain-space. Fast primitive was symmetrically distributed along the mid-line of the gain-space with equal variances along each axis, while the slow primitive is more aligned with the velocity axis in the space and had low correlation between the variances. The interaction of these two primitive spaces created similar pattern to subjects' behavior in position-dependent, velocity dependent, combination, and position-biased force-field environments.

### 3.5.1 Two Rates models of Motor Adaptation

The initial multi-rate model proposed by [3] has been implemented in multitude of motor adaptation paradigms. This model has been successful in explaining properties of motor adaptation including savings, anterograde interference and long term retention of the adaptation [3, 4, 61].

Although many of the effects are well described by this model, some studies have suggested that other processes might also be responsible for the adaptation behavior of the motor system. For instance, it has been suggested that adaptation might also accompanied by reinforcement learning mechanisms that are active in late phases of adaptation [7, 62].

The multi-rate state-dependent primitive model suggests that at least in force-field adaptation paradigms, the two populations of motion-dependent primitives with different time scale can capture both to inter trial force evolution as well as within trial. The behavior of the model replicated experimental data during both adaptation and unlearning of motion-dependent force-fields.

### 3.5.2 Asymmetries in the Primitive Distributions

A number of recent studies have shown that motion-dependent primitives are essential in explaining the different features of motion-dependent force-field adaptation. Sing et al. [5] was the first study to show the rate of learning can be well predicted by the overlap between the motion-dependency and the variance in the distribution of the primitives. On the other hand, experiencing a particular motion-dependent force-field can bias the subsequent force-field adaptation [36]. A more recent study shown that the initial variability in each primitive can predict the rate of adaptation to the force-field, and modulation of each primitive can increase the rate of subsequent adaptation [37]. Although the multi-rate state dependent model has not been tested these paradigms, we suspect that the rotation in the maximum variance direction can account for the result from both observations [36,37].

There is also evidence about the representation of movement kinematics in nervous system, including motor cortex, muscle spindles, and cerebellum. A number of recent studies have suggested that there can be a better representation of one motion variable over the others in some areas. For example, Paninski et al. [51] have shown that the velocity tuning is better in motor cortex areas compared to other movement kinematic variables. We speculate that the asymmetries in the primitive distribution is corollary to the degree of tuning to motion kinematics.

## Chapter 4:

### 4.1 Introduction

In this chapter we outlined 2 predations from multiple-rate state-dependent primitive model 2 novel force-field adaptation paradigms. We first analyzed the behavior of the model when the schedule of perturbation changed. We then predicted how the passage of time and subsequent re-exposure to force-field can refine the adaptation trajectory.

### 4.2 Prediction of Multi-rate State-dependent Primitive Model During Gradual Introduction of the Force-field

Throughout this thesis we assumed that the force-field was introduced as a step function after a baseline period. This type of force-field schedule, which we referred to as abrupt schedule, can introduce large error in motor output during early adaptation trials. A number of previous studies, however, introduced the force-field in a gradual manner in order to limit large errors [33,39]. Interestingly, the motor system adapted to this force-field in a gradual manner, and the final level of adaptation was comparable to abrupt schedule. Further, the multi-rate model could capture the changes in the adaptive behavior.

However, no study have explored whether the adaptation gain trajectories are different between abrupt and gradual schedule of the force-field. We showed that under abrupt schedule, the initial motor output contain goal-misaligned force-states that diminish with extended exposure. Given that the large errors were mainly present in initial phase of adaptation to abrupt force-field, we suspect that limiting this error could change the shape of adaptation trajectory. Specifically, initial adaptation would be more aligned with motion-dependency of the force-field. In order to test this prediction we simulated the multi-rate

state-dependent primitive model under gradual introduction of the force-field. After a baseline period, The force-field amplitude increased gradually until it reached the full scale (Eq. 4.1).

$$f(n) = \begin{cases} \frac{1}{15}n^x & n \leq 145 \\ 1 & n > 145 \end{cases} \quad \text{where : } x = \frac{\log(15)}{\log(145)} \quad (4.1)$$

After the adaptation period, the error was clamped to initiate the unlearning of motor adaptation. For a position-dependent force-field the goal of adaptation could be expressed as  $[0, f(n)]$  in gain-space. The multi-rate state-dependent primitive model response to the gradual position-dependent and velocity-dependent force-field is shown in Fig. 4.1.

The model showed that early adaptation no longer was biased towards the mid-line of the gain space. Instead it was closer to the goal aligned axis for both position-FF and velocity-FF. This specificity however came at a cost of reduced amount of initial learning. The unlearning two-state primitive model showed no systematical differences when compared to abrupt schedule.

### 4.3 Prediction of Multi-rate State-dependent Primitive Model During Extended Exposure to the Force-field

Unlearning of a motor memory can occur in two ways. When the motor system is actively engaged in the movement, either error clamp or null movement, the adaptation levels gradually reverts back to the baseline levels. This form of unlearning can be considered as experience-dependent unlearning. The other form of unlearning can occur when motor system is no longer performing the task. This type of unlearning is strictly dependent on time and can be referred to as temporal unlearning.

Joiner and Smith [4] have recently demonstrated that the temporal unlearning can be explained by the behavior of slow state in the multi-rate model. In their study subjects

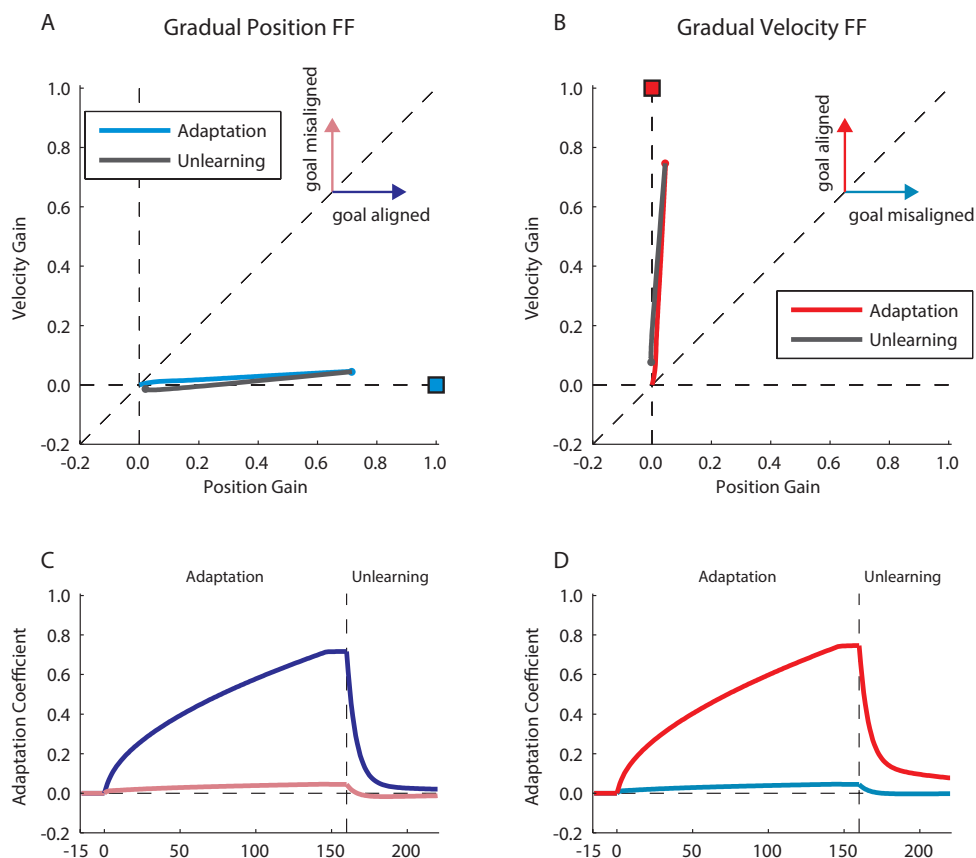


Figure 4.1: (A) Evolution of position and velocity gains during adaptation and unlearning of gradual Position-FF, gain trajectories during adaptation and unlearning periods are shown in blue and gray, respectively. The adaptation goal is shown as a blue filled rectangle. Each gain can be broken down to goal-aligned and goal misaligned components, as shown by two vectors. (B) Evolution of position and velocity gains during adaptation and unlearning of a velocity-FF. Adaptation gains are shown in red and unlearning gains in gray. Goal of adaptation is represented as a red square. Here direction of the goal aligned and goal misaligned components of each gain are shown as a red and cyan arrow, respectively. (C,D) The temporal changes for goal-aligned and goal-misaligned components are shown for each force field environment in A and B.

adapted to the velocity-dependent force-field with variable length in exposure period and retested in an error clamp environment 24 hours after initial adaptation in order to measure to memory of the force-field after the temporal unlearning. They showed that the level of motor memory was dependent on the initial length of force-field exposure. Furthermore, the motor memory of adaptation after 24 hours was always a scaled version of slow state adaptation level at the end of each force-field period.

Here we implemented the result from [4] to predict the change in the adaptation trajectory over multiple days of exposure to force-field. We simulated the multi-rate state-dependent primitive model in the following way. On the first day, after a small baseline period the model was exposed to a position-dependent force-field. At the end of force-field period, there was no longer any error clamp period. Instead the temporal unlearning was modeled by rescaling the weights for fast primitive back to zero, and the weights for slow state to 50% of their value at the end of adaptation period. This rescaling was comparable to the amount of retention observed previously. We also assumed that experiencing the force-field on the first day biases the distribution of the fast primitives towards position axis. As a result we reduce the  $\sigma_v^{fast}$  by 30%. For the second day, we introduced the same force-field environment which was then followed by an error-clamp unlearning period. Fig. 4.2 shows the behavior of the model under this paradigm.

The main observation here was the difference between the adaptation trajectories on the first and second day. The adaptation on the second day is more aligned to the motion-dependency of the force-field. In addition it seems to show the savings effect, where the rate of adaptation was faster upon re-exposure. Thus, the savings effect that has been previously reported force-field adaptation paradigms might be due to the increase in the specificity of adaptation trajectory. We will test this hypothesis in our future experiments.

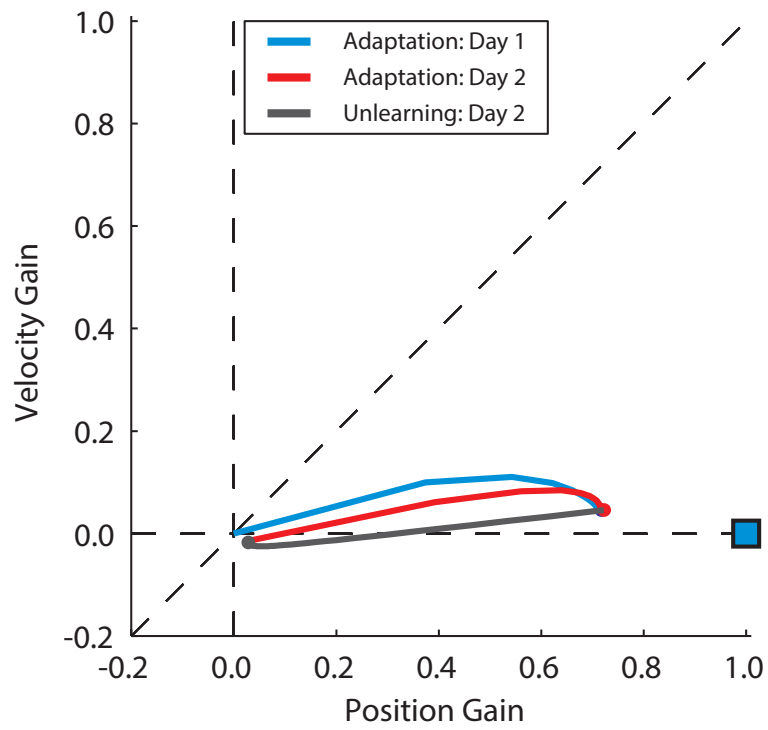


Figure 4.2: Gain trajectories during adaptation on the first and second days are shown in blue and red. Unlearning on the second day is shown by a gray solid line. The adaptation goal is shown as a blue filled square.



## Bibliography

## Bibliography

- [1] N. Bhushan and R. Shadmehr, “Computational nature of human adaptive control during learning of reaching movements in force fields,” *Biological cybernetics*, vol. 81, no. 1, pp. 39–60, 1999.
- [2] T. Poggio and E. Bizzi, “Generalization in vision and motor control,” *Nature*, vol. 431, no. 7010, pp. 768–774, 2004.
- [3] M. A. Smith, A. Ghazizadeh, and R. Shadmehr, “Interacting adaptive processes with different timescales underlie short-term motor learning,” *PLoS biology*, vol. 4, no. 6, p. e179, 2006.
- [4] W. M. Joiner and M. A. Smith, “Long-term retention explained by a model of short-term learning in the adaptive control of reaching,” *Journal of neurophysiology*, vol. 100, no. 5, pp. 2948–2955, 2008.
- [5] G. C. Sing, W. M. Joiner, T. Nanayakkara, J. B. Brayanov, and M. A. Smith, “Primitives for motor adaptation reflect correlated neural tuning to position and velocity,” *Neuron*, vol. 64, no. 4, pp. 575–589, 2009.
- [6] K. Wei, D. Wert, and K. Kording, “The nervous system uses nonspecific motor learning in response to random perturbations of varying nature,” *Journal of neurophysiology*, vol. 104, no. 6, pp. 3053–3063, 2010.
- [7] V. S. Huang, A. Haith, P. Mazzoni, and J. W. Krakauer, “Rethinking motor learning and savings in adaptation paradigms: model-free memory for successful actions combines with internal models,” *Neuron*, vol. 70, no. 4, pp. 787–801, 2011.
- [8] P. A. Vaswani and R. Shadmehr, “Decay of motor memories in the absence of error,” *The Journal of Neuroscience*, vol. 33, no. 18, pp. 7700–7709, 2013.
- [9] C. T. Noto and F. R. Robinson, “Visual error is the stimulus for saccade gain adaptation,” *Cognitive brain research*, vol. 12, no. 2, pp. 301–305, 2001.
- [10] Y.-w. Tseng, J. Diedrichsen, J. W. Krakauer, R. Shadmehr, and A. J. Bastian, “Sensory prediction errors drive cerebellum-dependent adaptation of reaching,” *Journal of Neurophysiology*, vol. 98, no. 1, pp. 54–62, 2007.
- [11] H. Chen-Harris, W. M. Joiner, V. Ethier, D. S. Zee, and R. Shadmehr, “Adaptive control of saccades via internal feedback,” *The Journal of Neuroscience*, vol. 28, no. 11, pp. 2804–2813, 2008.

- [12] M. Synofzik, A. Lindner, and P. Thier, “The cerebellum updates predictions about the visual consequences of one’s behavior,” *Current Biology*, vol. 18, no. 11, pp. 814–818, 2008.
- [13] S. E. Criscimagna-Hemminger, A. J. Bastian, and R. Shadmehr, “Size of error affects cerebellar contributions to motor learning,” *Journal of neurophysiology*, vol. 103, no. 4, pp. 2275–2284, 2010.
- [14] R. Shadmehr and F. A. Mussa-Ivaldi, “Adaptive representation of dynamics during learning of a motor task,” *The Journal of Neuroscience*, vol. 14, no. 5, pp. 3208–3224, 1994.
- [15] R. Miall and D. M. Wolpert, “Forward models for physiological motor control,” *Neural networks*, vol. 9, no. 8, pp. 1265–1279, 1996.
- [16] D. M. Wolpert, J. Diedrichsen, and J. R. Flanagan, “Principles of sensorimotor learning,” *Nature Reviews Neuroscience*, vol. 12, no. 12, pp. 739–751, 2011.
- [17] J. Diedrichsen, “Dissociating timing and coordination as functions of the cerebellum.”
- [18] T. Martin, J. Keating, H. Goodkin, A. Bastian, and W. Thach, “Throwing while looking through prisms ii. specificity and storage of multiple gazethrow calibrations,” *Brain*, vol. 119, no. 4, pp. 1199–1211, 1996.
- [19] J. Fernandez-Ruiz, R. Diaz, C. Aguilar, and C. Hall-Haro, “Decay of prism aftereffects under passive and active conditions,” *Cognitive brain research*, vol. 20, no. 1, pp. 92–97, 2004.
- [20] C. Gordon, W. Fletcher, G. M. Jones, and E. Block, “Adaptive plasticity in the control of locomotor trajectory,” *Experimental Brain Research*, vol. 102, no. 3, pp. 540–545, 1995.
- [21] T. Prokop, W. Berger, W. Zijlstra, and V. Dietz, “Adaptational and learning processes during human split-belt locomotion: interaction between central mechanisms and afferent input,” *Experimental brain research*, vol. 106, no. 3, pp. 449–456, 1995.
- [22] K. Weber, W. Fletcher, C. Gordon, G. M. Jones, and E. Block, “Motor learning in the podokinetic system and its role in spatial orientation during locomotion,” *Experimental brain research*, vol. 120, no. 3, pp. 377–385, year=.
- [23] D. S. Reisman, H. J. Block, and A. J. Bastian, “Interlimb coordination during locomotion: what can be adapted and stored?” *Journal of neurophysiology*, vol. 94, no. 4, pp. 2403–2415, 2005.
- [24] J. W. Krakauer, C. Ghez, and M. F. Ghilardi, “Adaptation to visuomotor transformations: consolidation, interference, and forgetting,” *The Journal of Neuroscience*, vol. 25, no. 2, pp. 473–478, 2005.
- [25] L. Shmuelof, V. S. Huang, A. M. Haith, R. J. Delnicki, P. Mazzoni, and J. W. Krakauer, “Overcoming motor forgetting through reinforcement of learned actions,” *The Journal of Neuroscience*, vol. 32, no. 42, pp. 14 617–14 621a, 2012.

- [26] T. Kitago, S. L. Ryan, P. Mazzoni, J. W. Krakauer, and A. M. Haith, “Unlearning versus savings in visuomotor adaptation: comparing effects of washout, passage of time, and removal of errors on motor memory,” *Frontiers in human neuroscience*, vol. 7, 2013.
- [27] R. Shadmehr and T. Brashers-Krug, “Functional stages in the formation of human long-term motor memory,” *The Journal of Neuroscience*, vol. 17, no. 1, pp. 409–419, 1997.
- [28] P. J. Cordo, “Mechanisms controlling accurate changes in elbow torque in humans,” *The Journal of neuroscience*, vol. 7, no. 2, pp. 432–442, 1987.
- [29] P. Cordo, “Kinesthetic control of a multijoint movement sequence,” *J Neurophysiol*, vol. 63, no. 1, pp. 161–72, 1990.
- [30] M. J. Wagner and M. A. Smith, “Shared internal models for feedforward and feedback control,” *The Journal of Neuroscience*, vol. 28, no. 42, pp. 10 663–10 673, 2008.
- [31] R. A. Scheidt, D. J. Reinkensmeyer, M. A. Conditt, W. Z. Rymer, and F. A. Mussa-Ivaldi, “Persistence of motor adaptation during constrained, multi-joint, arm movements,” *Journal of Neurophysiology*, vol. 84, no. 2, pp. 853–862, 2000.
- [32] S. E. Criscimagna-Hemminger and R. Shadmehr, “Consolidation patterns of human motor memory,” *The Journal of Neuroscience*, vol. 28, no. 39, pp. 9610–9618, 2008.
- [33] V. S. Huang and R. Shadmehr, “Persistence of motor memories reflects statistics of the learning event,” *Journal of neurophysiology*, vol. 102, no. 2, pp. 931–940, 2009.
- [34] S. E. Pekny, S. E. Criscimagna-Hemminger, and R. Shadmehr, “Protection and expression of human motor memories,” *The Journal of Neuroscience*, vol. 31, no. 39, pp. 13 829–13 839, 2011.
- [35] G. C. Sing, S. P. Orozco, and M. A. Smith, “Limb motion dictates how motor learning arises from arbitrary environmental dynamics,” *Journal of neurophysiology*, vol. 109, no. 10, pp. 2466–2482, 2013.
- [36] N. Yousif and J. Diedrichsen, “Structural learning in feedforward and feedback control,” *Journal of neurophysiology*, vol. 108, no. 9, pp. 2373–2382, 2012.
- [37] H. G. Wu, Y. R. Miyamoto, L. N. G. Castro, B. P. Olveczky, and M. A. Smith, “Temporal structure of motor variability is dynamically regulated and predicts motor learning ability,” *Nature neuroscience*, 2014.
- [38] W. M. Joiner, O. Ajayi, G. C. Sing, and M. A. Smith, “Linear hypergeneralization of learned dynamics across movement speeds reveals anisotropic, gain-encoding primitives for motor adaptation,” *Journal of neurophysiology*, vol. 105, no. 1, pp. 45–59, 2011.
- [39] W. M. Joiner, J. B. Brayanov, and M. A. Smith, “The training schedule affects the stability, not the magnitude, of the interlimb transfer of learned dynamics,” *Journal of neurophysiology*, vol. 110, no. 4, pp. 984–998, 2013.

- [40] L. N. Gonzalez Castro, A. M. Hadjiosif, M. A. Hemphill, and M. A. Smith, “Environmental consistency determines the rate of motor adaptation,” *Current Biology*, vol. 24, no. 10, pp. 1050–1061, 2014.
- [41] A. E. Brennan and M. A. Smith, “Immediate decay onset in fixed and variable environments,” *Proceedings of translational and computational motor control*, vol. Nov. 8, 2013.
- [42] J. N. Ingram, J. R. Flanagan, and D. M. Wolpert, “Context-dependent decay of motor memories during skill acquisition,” *Current Biology*, vol. 23, no. 12, pp. 1107–1112, 2013.
- [43] M. Shidara, K. Kawano, H. Gomi, and M. Kawato, “Inverse-dynamics model eye movement control by purkinje cells in the cerebellum,” 1993.
- [44] R. Soetedjo and A. F. Fuchs, “Complex spike activity of purkinje cells in the oculomotor vermis during behavioral adaptation of monkey saccades,” *The Journal of neuroscience*, vol. 26, no. 29, pp. 7741–7755, 2006.
- [45] Q.-G. Fu, D. Flament, J. Coltz, and T. Ebner, “Relationship of cerebellar purkinje cell simple spike discharge to movement kinematics in the monkey,” *Journal of Neurophysiology*, vol. 78, no. 1, pp. 478–491, 1997.
- [46] A. V. Roitman, S. Pasalar, M. T. Johnson, and T. J. Ebner, “Position, direction of movement, and speed tuning of cerebellar purkinje cells during circular manual tracking in monkey,” *The Journal of neuroscience*, vol. 25, no. 40, pp. 9244–9257, 2005.
- [47] S. Pasalar, A. Roitman, W. Durfee, and T. Ebner, “Force field effects on cerebellar purkinje cell discharge with implications for internal models,” *Nature neuroscience*, vol. 9, no. 11, pp. 1404–1411, 2006.
- [48] A. L. Hewitt, L. S. Popa, S. Pasalar, C. M. Hendrix, and T. J. Ebner, “Representation of limb kinematics in purkinje cell simple spike discharge is conserved across multiple tasks,” *Journal of neurophysiology*, vol. 106, no. 5, pp. 2232–2247, 2011.
- [49] A. P. Georgopoulos, J. F. Kalaska, R. Caminiti, and J. T. Massey, “On the relations between the direction of two-dimensional arm movements and cell discharge in primate motor cortex,” *The Journal of Neuroscience*, vol. 2, no. 11, pp. 1527–1537, 1982.
- [50] D. W. Moran and A. B. Schwartz, “Motor cortical representation of speed and direction during reaching,” *Journal of Neurophysiology*, vol. 82, no. 5, pp. 2676–2692, 1999.
- [51] L. Paninski, M. R. Fellows, N. G. Hatsopoulos, and J. P. Donoghue, “Spatiotemporal tuning of motor cortical neurons for hand position and velocity,” *Journal of neurophysiology*, vol. 91, no. 1, pp. 515–532, 2004.
- [52] J. F. Kalaska, D. Cohen, M. L. Hyde, and M. Prud’Homme, “A comparison of movement direction-related versus load direction-related activity in primate motor cortex, using a two-dimensional reaching task,” *The Journal of neuroscience*, vol. 9, no. 6, pp. 2080–2102, 1989.

- [53] W. Truccolo, G. M. Friehs, J. P. Donoghue, and L. R. Hochberg, “Primary motor cortex tuning to intended movement kinematics in humans with tetraplegia,” *The Journal of Neuroscience*, vol. 28, no. 5, pp. 1163–1178, 2008.
- [54] S. Wise, S. Moody, K. Blomstrom, and A. Mitz, “Changes in motor cortical activity during visuomotor adaptation,” *Experimental Brain Research*, vol. 121, no. 3, pp. 285–299, 1998.
- [55] F. Gandolfo, C.-S. Li, B. Benda, C. P. Schioppa, and E. Bizzi, “Cortical correlates of learning in monkeys adapting to a new dynamical environment,” *Proceedings of the National Academy of Sciences*, vol. 97, no. 5, pp. 2259–2263, 2000.
- [56] C.-S. R. Li, C. Padoa-Schioppa, and E. Bizzi, “Neuronal correlates of motor performance and motor learning in the primary motor cortex of monkeys adapting to an external force field,” *Neuron*, vol. 30, no. 2, pp. 593–607, 2001.
- [57] J. Xiao, C. Padoa-Schioppa, and E. Bizzi, “Neuronal correlates of movement dynamics in the dorsal and ventral premotor area in the monkey,” *Experimental brain research*, vol. 168, no. 1-2, pp. 106–119, 2006.
- [58] W. Wang, S. S. Chan, D. A. Heldman, and D. W. Moran, “Motor cortical representation of position and velocity during reaching,” *Journal of neurophysiology*, vol. 97, no. 6, pp. 4258–4270, 2007.
- [59] J. M. Galea, A. Vazquez, N. Pasricha, J.-J. O. de Xivry, and P. Celnik, “Dissociating the roles of the cerebellum and motor cortex during adaptive learning: the motor cortex retains what the cerebellum learns,” *Cerebral Cortex*, vol. 21, no. 8, pp. 1761–1770, 2011.
- [60] D. J. Herzfeld, D. Pastor, A. M. Haith, Y. Rossetti, R. Shadmehr, and J. O’Shea, “Contributions of the cerebellum and the motor cortex to acquisition and retention of motor memories,” *NeuroImage*, 2014.
- [61] G. C. Sing and M. A. Smith, “Reduction in learning rates associated with anterograde interference results from interactions between different timescales in motor adaptation,” *PLoS computational biology*, vol. 6, no. 8, p. e1000893, 2010.
- [62] A. M. Haith and J. W. Krakauer, “Model-based and model-free mechanisms of human motor learning,” in *Progress in Motor Control*. Springer, 2013, pp. 1–21.

## Curriculum Vitae

Eghbal Hosseini Asl graduated from received his Bachelor of Science in Electrical Engineering from Iran University of Science and Tech. Tehran, Iran, in 2010. Since January 2012, he has been pursuing his Masters in Electrical Engineering at George Mason University, Fairfax, VA. His main area of interests are sensorimotor integration and motor adaptation in central nervous system.